



Cite this: *Org. Biomol. Chem.*, 2018, **16**, 6206

## Molecular tweezers with a rotationally restricted linker and freely rotating porphyrin moieties†

Rhys B. Murphy, <sup>‡a</sup> Duc-Truc Pham, <sup>b</sup> Jonathan M. White, <sup>c</sup> Stephen F. Lincoln <sup>b</sup> and Martin R. Johnston <sup>\*a</sup>

The effect of the degree of conformational rigidity and/or flexibility on preorganisation in artificial molecular receptors continues to be actively explored by supramolecular chemists. This work describes a bis-porphyrin architecture, linked via a rigid polycyclic backbone, in which a sterically bulky 2,3,5,6-tetramethylphenyl diimide core restricts rotation to afford two non-interconvertible tweezer conformations; *syn*- and *anti*-. After separation, the host–guest chemistry of each conformation was studied independently. The difference in host geometry allows only the *syn*-conformation to form a strong 1 : 1 bis-porphyrin complex with the diamino ligand 1,4-diazabicyclo[2.2.2]octane (DABCO) ( $K_{11} = 1.25 \times 10^8 \text{ M}^{-1}$ ), with the *anti*-conformation adopting a 2 : 2 sandwich complex with DABCO ( $K_{22} = 5.57 \times 10^{17} \text{ M}^{-3}$ ).

Received 22nd April 2018,  
Accepted 23rd July 2018

DOI: 10.1039/c8ob00944a

rsc.li/obc

## Introduction

The guest complexation behavior of molecular tweezers is heavily dependent on the crucial role played by the linker in providing preorganisation.<sup>1–3</sup> In general terms, it is reported that conformationally rigid linkers afford larger association constants than systems with conformationally flexible linkers,<sup>4,5</sup> as well as offering substrate selectivity provided that the dimensions of the tweezer cavity are suited to the substrate.<sup>4</sup> Conformationally flexible linkers allow complexation of substrates of different sizes and shapes,<sup>4,6</sup> and these systems may suffer from poor selectivity.<sup>7</sup> However, it can be advantageous to balance the degree of host preorganisation and rigidity with conformational flexibility, as demonstrated by several notable examples:

- a metallocporphyrin host which increases the rate of a hetero-Diels–Alder reaction,<sup>8</sup>
- disulfide-linked bis(cyclopeptides) which display high affinity and selectivity for the sulfate anion in aqueous solution,<sup>9</sup>

● the comparison of the effective molarities (EM) for a large number of porphyrin-pyridine complexes with different torsional degrees of freedom,<sup>10</sup>

● and the use of flexible cyclodextrins to template porphyrin nanorings.<sup>11</sup>

In a series of bis-porphyrin hosts each containing different linker structures,<sup>12–14</sup> it has been observed that large association constants can be obtained for architectures containing either conformationally flexible, restricted, or more rigidly constrained linkers, and that the linker need only confer the system with moderate preorganization. § Additional evidence for this is provided by both our recent work<sup>15</sup> and a variety of porphyrin host–guest systems with varying degrees of preorganisation,<sup>6–8,12,13,16–27</sup> including those which allow defined changes in interporphyrin distance. Further, there continues to be an active interest to explore linker conformational rigidity/flexibility in porphyrin tweezers.<sup>28,29</sup>

Biological receptors, which are dynamic and far from rigid, possess comparatively larger association constants compared to those of most artificial receptors.<sup>5,9</sup> This has led to discussion that adopting a rigid-only approach to host design which relies solely on covalent linkages to establish geometry could limit the scope of artificial receptors.<sup>5,9</sup>

We have previously described the host–guest chemistry of bis-porphyrin tweezer **1**,<sup>15</sup> which forms a strong 1 : DABCO bis-porphyrin:DABCO complex with the aliphatic diamino ligand 1,4-diazabicyclo[2.2.2]octane (DABCO), and more recently reported the synthesis of a tetra-porphyrin tweezer **2**

<sup>a</sup>Flinders Centre for NanoScale Science and Technology, College of Science and Engineering, Flinders University, Bedford Park, Adelaide, Australia.

E-mail: martin.johnston@flinders.edu.au

<sup>b</sup>Department of Chemistry, The University of Adelaide, Adelaide, Australia

<sup>c</sup>School of Chemistry, The University of Melbourne, Melbourne, Australia

† Electronic supplementary information (ESI) available: NMR, UV/Vis, MS, X-ray, complexation models, statistical analysis, effective molarity. CCDC 1526930 and 1526931. For ESI and crystallographic data in CIF or other electronic format see DOI: 10.1039/c8ob00944a

‡ Present address: Australian Nuclear Science and Technology Organisation, Locked Bag 2001, Kirrawee DC, NSW 2232, Australia.

§ Although there are examples where conformationally flexible linkers are insufficiently preorganised and small association constants are obtained.<sup>13,14</sup>



with two cooperative binding sites<sup>30</sup> (Fig. 1). In these systems, host preorganisation was achieved by using a bridged polycyclic linker. The favourable properties of fused [n]polynorbornyl scaffolds in molecular receptors, particularly with respect to host preorganisation, are reported in the literature by a number of research groups including those of Warrener and Butler,<sup>7,31–39</sup> Paddon-Row,<sup>40–43</sup> Johnston,<sup>19,44–46</sup> Pfeffer,<sup>47–53</sup> Clever,<sup>47,50,54</sup> and Margetić.<sup>55–58</sup>

Importantly, tweezers **1** and **2** share a freely rotating phenyl diimide core inserted within the otherwise rigid polycyclic linker, a feature which allows unhindered adjustment of the interporphyrin distance, to potentially allow the binding of guests of different lengths. However, because all conformations are readily accessible, the possibility of **1** assuming an *anti*-conformation arises, thereby decreasing the proportion of the *syn*-conformation and the formation of *syn*-**1** bis-porphyrin:guest complexes. This possibility is also inherent in the design of other molecular tweezers in the literature (for several examples see ref. 24 and 59–63).

To investigate the role of the phenyl core on the host-guest behaviour of molecular architectures **1** and **2**, we designed restricted rotation tweezer **3** (Fig. 2). Tweezer **3** maintains the rigid bridged polycyclic scaffold but contains a phenyl diimide core with sterically bulky methyl substituents (dotted box, Fig. 2). These methyl substituents drastically increase the energy barrier to rotation about the phenyl diimide core and afford non-interconvertible *syn*-**3a** and *anti*-**3b** conformations, providing the opportunity to study the host-guest complexation of each conformation independently.

This manuscript reports on the synthesis, isolation and characterisation of the *syn*-**3a** and *anti*-**3b** conformers. Further,

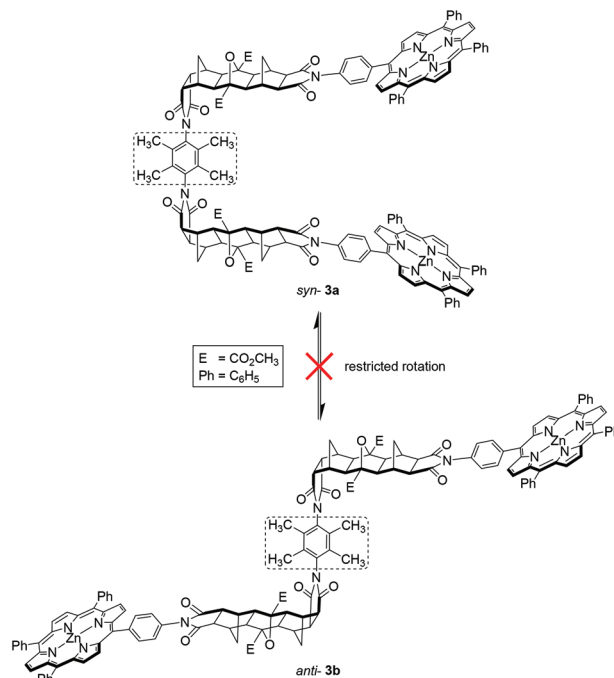


Fig. 2 Restricted rotation single binding site tweezer **3**, where non-interconvertible *syn*-**3a** and *anti*-**3b** conformations arise due to a sterically bulky 2,3,5,6-tetramethylphenyl diimide core.

their complexation with DABCO was studied by UV-Vis and NMR spectroscopy and the resulting data fitted to various models of stoichiometry using non-linear least squares analysis.

## Results and discussion

### Synthesis

The synthesis of tweezer **3** was undertaken in a similar manner to tweezer **1**<sup>15</sup> involving the condensation of *endo*-Mitsudo anhydride **4**<sup>15,55</sup> with 2,3,5,6-tetramethyl-*p*-phenylenediamine **5**, followed by ring closing to form imides **6a** and **6b** (Scheme 1).

The <sup>1</sup>H NMR spectrum of the reaction mixture (not shown) revealed two pairs of signals for the methyl phenyl substituent proton resonances. This was attributed to the two different linker conformations of *syn*-**6a** and *anti*-**6b**. The mixture showed a slight deviation from statistical, in an approximately 60 : 40 ratio based on the relative integration between the two pairs of signals within the mixture.¶

To provide experimental evidence for separate *syn*-**6a** and *anti*-**6b** conformers, a small sample was separated by using a combination of column chromatography and selective recrystallisation. The partial <sup>1</sup>H NMR spectra highlighting the

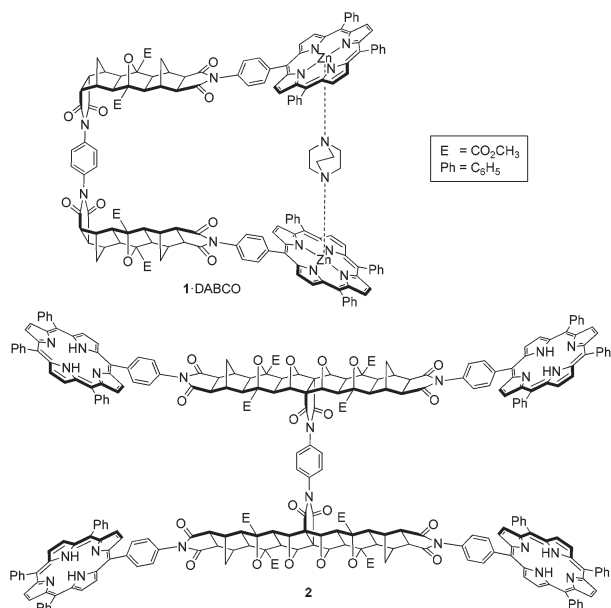
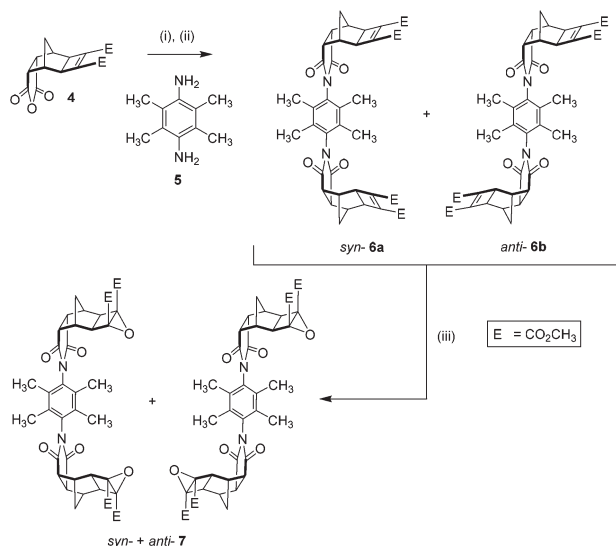


Fig. 1 Previously described tweezer systems with a freely rotating phenyl diimide core; single binding site tweezer **1**<sup>15</sup> (shown as complex **1**:DABCO), and two binding site tweezer **2**.<sup>30</sup>

¶ This apparent non-statistical mixture could result from differential solubility of the *syn*-**6a** and *anti*-**6b** conformations in the precipitate and filtrate after the reaction, however this has not been investigated further.





**Scheme 1** Synthesis of the restricted rotation linker. (i) 2,3,5,6-Tetramethyl-*p*-phenylenediamine **5** (0.5 eq.), dry DMSO, Ar deoxygenated, 80 °C, 1 day; (ii) NaOAc/Ac<sub>2</sub>O, 80 °C, 1 day, 72% (as a mixture of *syn*-**6a** + *anti*-**6b**); (iii) anhydrous *t*BuOOH in toluene (3.3 M, 2.5–5 eq.), dry CH<sub>2</sub>Cl<sub>2</sub>, 0 °C, 10 min, *t*BuOK (1–2 eq.), room temp., 3.5–7 h, 51%.

methyl resonances are shown in Fig. 3 (full <sup>1</sup>H NMR spectra S1 and S3†). In either conformation, the two methyl groups are non-equivalent resulting in two resonances. Additionally, the *syn*-**6a** and *anti*-**6b** conformations have different <sup>13</sup>C NMR spectra (S2 and S4†); with pairs of non-equivalent methyl and phenyl carbon resonances evident.

The mixture of *syn*-**6a** and *anti*-**6b** was subsequently epoxidised under standard conditions for electron deficient alkenes

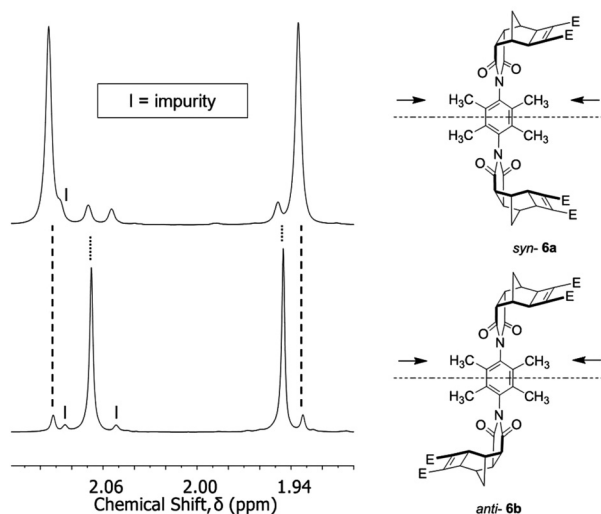
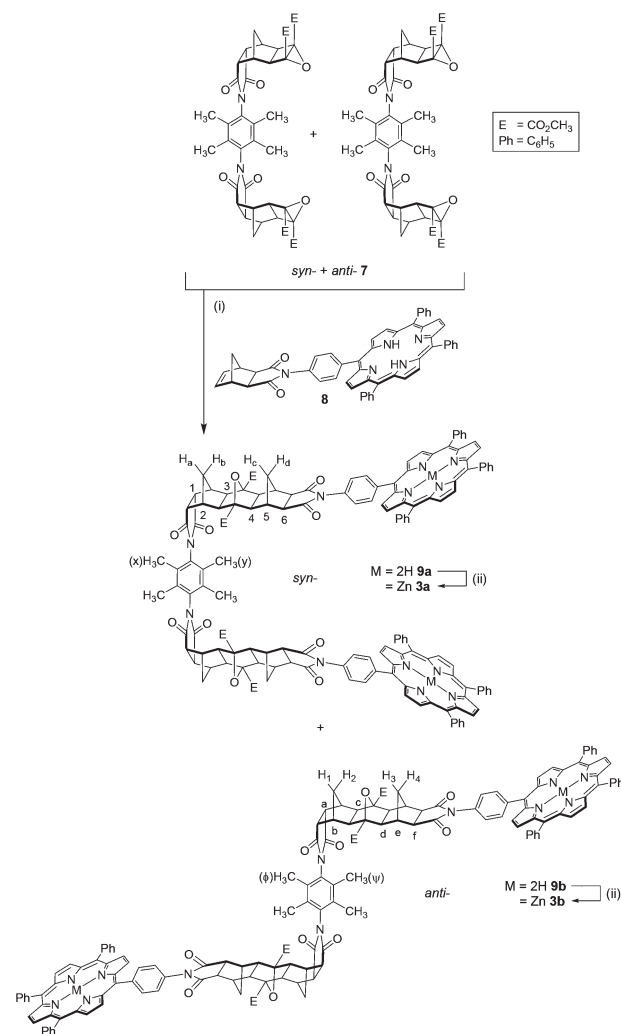


**Fig. 3** Selected region of the <sup>1</sup>H NMR spectrum of the *syn*-**6a** and *anti*-**6b** restricted rotation linker (absolute conformation unassigned), showing the different chemical environments of the methyl groups. Each sample contained traces of the other conformation and these are shown by the dotted lines. Impurity is marked by the letter I. Spectra recorded at 600 MHz in CDCl<sub>3</sub>.

(*t*BuOOH/*t*BuOK)<sup>33,35</sup> to afford bis-epoxide **7** (Scheme 1). The bis-epoxide mixture **7** was subsequently appended with *exo*-porphyrin receptors **8**<sup>15</sup> via the alkene plus cyclobutane epoxide (ACE) reaction (Scheme 2) in a sealed tube.<sup>64</sup> Overall, the reaction proceeded in a 23% yield, which upon NMR analysis was shown to exist as 10% *syn*-**9a** and 13% *anti*-**9b** conformations. The *syn*- and *anti*-assignment was achieved using <sup>1</sup>H NMR of the zinc metallated porphyrin derivatives, **3a** and **3b** respectively (*vide infra*).

The <sup>1</sup>H NMR spectra of the *syn*-**9a** and *anti*-**9b** mixture contained several features characteristic of ACE-coupled reactions, including a small downfield shift for the methyl ester resonance compared to that of the epoxide **7**,<sup>65</sup> along with the disappearance of the norbornyl proton resonance from the *exo*-porphyrin receptor **8** at 6.45 ppm. The <sup>13</sup>C NMR spectrum contained a resonance at 90 ppm, similar to other polycyclic



**Scheme 2** Synthesis of tweezer **3**, *syn*-**3a** and *anti*-**3b**. (i) *exo*-Porphyrin receptor **8** (2 eq.), dry THF, sealed tube, 160 °C, 24 h, 23% (10% *syn*-**3a** + 13% *anti*-**3b**); (ii) Zn(OAc)<sub>2</sub>/MeOH/CHCl<sub>3</sub>, reflux, 1–2 h, 79–89%.



systems,<sup>38</sup> which is assigned to the bridgehead carbon atoms in the newly formed 7-oxanorbornane.<sup>38</sup>

Relative integration of the two inner pyrrole proton resonances in the <sup>1</sup>H NMR spectrum of the crude mixture suggested the ratio of *syn*-: *anti*- was approximately 43 : 57. While separation by column chromatography yielded the *anti*-**9b** conformation completely free of *syn*-**9a**, the *syn*-**9a** conformation contained approximately 25% residual *anti*-**9b**. In an effort to conserve limited product, further purification to remove *anti*-**9b** from *syn*-**9a** was carried out post-zinc(II) metallation, as *syn*-**3a**. The identity of the partially purified freebase *syn*-**9a** and *anti*-**9b** were confirmed by using accurate MS (S9),<sup>†</sup> ESI-TOF, for two samples containing different ratios of *syn*-**9a** and *anti*-**9b** (sample 1 [M + 2H]<sup>2+</sup> found: 1162.4267, calc: 1162.4260; sample 2 [M + 2Na]<sup>2+</sup> found: 1184.4110, calc: 1184.4079).

The freebase *syn*-**9a** and *anti*-**9b** mixture and pure *anti*-**9b** were metallated with zinc(II) under standard conditions,<sup>66</sup> giving *syn*-**3a** and *anti*-**3b** respectively (Scheme 2). Zinc(II) metallation was characterised by loss of the porphyrin inner pyrrole proton resonance at −2.80 (*anti*-) and −2.84 (*syn*-) in the <sup>1</sup>H NMR spectrum. Several slow recrystallisations enabled the zinc(II) *syn*-**3a** conformation to be purified completely free of *anti*-**3b**. HRMS (MALDI-TOF) of *syn*-**3a** and *anti*-**3b** further confirmed zinc(II) metallation. MALDI-TOF of porphyrin compounds is reported to afford the radical molecular ion, [M]<sup>•+</sup>, without the uptake of H<sup>+</sup> or Na<sup>+</sup>.<sup>67</sup> The monoisotopic mass for [M]<sup>•+</sup> was found to be 2446.694 for *syn*-**3a** and 2446.6770 for *anti*-**3b**, which compares well with the calculated value of 2446.6644 (5,10,15,20-tetraphenylporphyrin, H<sub>2</sub>TPP, was used for internal calibration). In addition, the profiles of the experimental and theoretical MS spectra are in excellent agreement (S15<sup>†</sup>).

In the <sup>1</sup>H NMR spectrum for each adduct (*syn*-**3a**, S10,<sup>†</sup> *anti*-**3b**, S13<sup>†</sup>), ten polycyclic resonances occur as expected (excluding the methyl ester and two methyl phenyl substituent resonances); six singlets and four doublets. The doublets arise from two pairs of non-equivalent methylene bridge protons, H<sub>a</sub>/H<sub>b</sub> and H<sub>c</sub>/H<sub>d</sub> in the case of *syn*-**3a**, and H<sub>1</sub>/H<sub>2</sub> and H<sub>3</sub>/H<sub>4</sub> in the case of *anti*-**3b** (Scheme 2). These pairs (e.g. H<sub>a/b</sub> and H<sub>c/d</sub>, or H<sub>1/2</sub> and H<sub>3/4</sub>) appear at significantly different chemical shifts, characteristic of steric compression by oxygen in these systems,<sup>55</sup> and confirms the formation of a linear ACE product.<sup>55</sup> These resonances occur at chemical shifts of 2.77/1.43 ppm and 2.49/1.13 ppm for *syn*-**3a** and 2.77/1.42 ppm and 2.54/1.22 ppm for *anti*-**3b**. The six signals correspond with the number of unique proton chemical environments along the polycyclic scaffold (marked 1–6 for *syn*-**3a** and a–f for *anti*-**3b** in Scheme 2). In addition, a pair of methyl phenyl substituent resonances for the linker core are observed at chemical shifts of 2.31 and 2.00 ppm for *syn*-**3a** and 2.28 and 2.04 ppm for *anti*-**3b** (marked x and y for *syn*-**3a**, Φ and Ψ for *anti*-**3b** in Scheme 2, absolute assignment not determined). This is in line with similar observations for the *syn*-**6a** and *anti*-**6b** linkers described in Fig. 3.

The different aromatic regions of the <sup>1</sup>H NMR spectra of *syn*-**3a** and *anti*-**3b** are shown in Fig. 4. The splitting of the porphyrin resonances, in particular the β-pyrrole resonances, and the differences in integration of the *meso*-phenyl resonances between the two conformations indicates facial differentiation of the porphyrin macrocycles as a result of the close proximity of the opposing ring in the *syn*-conformation. For the *anti*-conformation, no major splitting of the porphyrin resonances was observed and the integrations are typical of compounds of the type mono-porphyrin **10**<sup>15</sup> (structure given in Table 1), presumably as the porphyrins cannot be positioned cofacially (unless intermolecular aggregation occurs). Additionally, the *syn*-conformation porphyrin resonances are shielded relative to the *anti*-, further demonstrating the effect of the adjacent π systems in the *syn*-conformation.

For the *syn*-**3a** tweezer, several of the porphyrin *meso*-phenyl <sup>1</sup>H NMR resonances are broadened while others appear sharp. Furthermore, the <sup>1</sup>H NMR spectrum was highly concentration dependent (S12(a)<sup>†</sup>), with significant resonance shifts observed for porphyrin and polycyclic resonances (Δδ = 0.3–0.7 ppm for samples more and less concentrated than 3.5 mM). Additional resonance shifts are observed between +20 °C and −50 °C (S12(b)<sup>†</sup>). Taken together, these data suggest that the *syn*-tweezer is undergoing dynamic conformational changes (but not to *anti*-) on the NMR timescale,

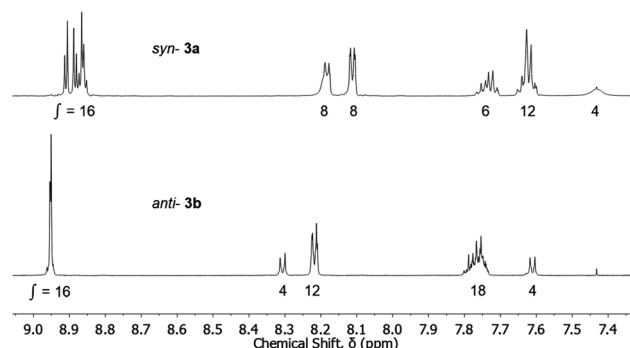
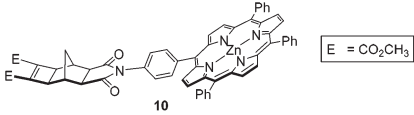


Fig. 4 Partial <sup>1</sup>H NMR (aromatic region) of the zinc(II) metallated *syn*-**3a** and *anti*-**3b** restricted rotation tweezers. Spectra recorded at 600 MHz in CDCl<sub>3</sub>.

Table 1 Summary of UV/Vis data in chloroform comparing *syn*-**3a** and *anti*-**3b** with mono-porphyrin **10** and tweezer **1**

| Species                 |  |   |                                 |                                  |
|-------------------------|--|---|---------------------------------|----------------------------------|
|                         | Zinc(II) mono-porphyrin <b>10</b> <sup>15</sup>                                      | Zinc(II) freely rotating <b>1</b> <sup>15</sup> | Zinc(II) <i>syn</i> - <b>3a</b> | Zinc(II) <i>anti</i> - <b>3b</b> |
| λ <sub>max</sub> (nm)   | 419.3  | 419.5   | 418.4                           | 419.3                            |
| Width (nm) <sup>a</sup> | 9.9  | 11.0  | 11.5                            | 10.1                             |

<sup>a</sup> Peak bandwidth measured at half height.





and/or changes to intermolecular aggregation influenced by concentration and temperature, however this has not been investigated further.

For the zinc(II) *anti*-**3b** adduct, there are only minor (<0.1 ppm) shifts in the spectrum at –50 °C compared to room temperature. Concentration dependence of the <sup>1</sup>H NMR could not be established for *anti*-**3b** due to poor solubility at concentrations greater than 0.85 mM.

The UV/Vis spectra of the zinc(II) metallated *syn*-**3a** and *anti*-**3b** adducts supported our conformational assignment. Zinc(II) *anti*-**3b** and zinc(II) mono-porphyrin **10**<sup>15</sup> display very similar Soret maxima and peak bandwidths at half height (Table 1). The absence of exciton coupling interactions supports the assignment of the *anti*-conformation,<sup>59</sup> where the bis-porphyrins are not positioned cofacially. Conversely, the Soret maxima of the zinc(II) *syn*-**3a** tweezer is blue shifted by 1 nm relative to the zinc(II) mono-porphyrin **10**, and has a slightly larger peak bandwidth at half height than the zinc(II) freely rotating tweezer **1** (Table 1). Although the blue shift and broadening of the Soret band are both small, this could indicate weak exciton coupling interactions<sup>19,22,59,68–72</sup> between the porphyrins in the *syn*-**3a** adduct. The weakness of the exciton coupling in the *syn*-**3a** adduct suggests that the bis-porphyrins are not fixed in a cofacial orientation, and that the porphyrin units are able to undergo rotation either about the *meso*-phenyl linking the porphyrin to the scaffold, and/or the two porphyrin arms can undergo restricted rotation about the diimide core.

## 2,3,5,6-Tetramethylphenyl diimide as the linker

Restricted rotation has been reported for *N*-phenyl imide derivatives with *ortho*-substituents other than hydrogen.<sup>73–83,94</sup> As the size of this substituent increases, the energy barrier to rotation increases due to steric repulsion with the oxygen atom of the imide.<sup>84–86</sup> In addition, the angle between the substituted phenyl and imide rings increases towards perpendicular to minimise this steric interaction.<sup>84,85,87,88</sup> This comes at the expense of resonance delocalisation and conjugation favoured in the planar conformation<sup>89,90</sup>.

NMR studies for mono-*ortho*-methyl substituted *N*-phenyl imide derivatives<sup>73,74</sup> report a mixture of rotational isomers at ambient conditions and which undergo thermally activated bond rotation. No interconversion between *syn*-**3a** and *anti*-**3b** was observed for our fully substituted 2,3,5,6-tetramethylphenyl 1,4-diimide under the conditions examined; the systems are both stable to interconversion at room temperature over the duration of NMR experiments, while the <sup>1</sup>H NMR spectrum of the pure *anti*-**3b** adduct after microwave irradiation at 95 °C for 15 minutes (300 W, 50 psi), or sonication at 30 °C for 15 minutes, showed no detectable interconversion from *anti*-**3b** to *syn*-**3a** (higher temperatures and longer times were not explored). However, a range of intermediate

conformations are envisaged to be energetically accessible within each of *syn*-**3a** and *anti*-**3b**, and would allow for some adjustment of the interporphyrin distance in the presence of guest.

Furthermore, in the course of this work, we examined several variations of linker **6**,<sup>90</sup> most notably the *exo*-analogues **11** (Fig. 5). During synthesis of **11**, the crude filtrate and crude precipitate of the reaction mixture contained mainly the opposite conformational isomer respectively (different solubility). Conveniently, slow evaporation of acetonitrile solutions of the precipitate and filtrate afforded crystals suitable for X-ray diffraction measurements. The crystal structures are shown in Fig. 6.

While crystal packing forces must be considered, these crystal structures provide unequivocal evidence supporting the formation of distinct *syn*-**11a** and *anti*-**11b** conformations (Fig. 6(a) and (b) respectively). Key parameters for the X-ray crystallographic measurements are provided in S18 and S21.†

An interesting structural feature revealed in Fig. 6 is the noticeable deviation of the 2,3,5,6-tetramethylphenyl core from planarity (view 2). The *syn*-**11a** conformation is co-crystallised with acetonitrile solvent, while the *anti*-**11b** conformation is co-crystallised with approximately 6% of a mono-epoxide impurity.

The presence of co-crystallised epoxide for *anti*-**11b** was unexpected, and re-examination of the high resolution mass spectrometry for samples prior to crystallisation revealed a second signal in the mass spectra of both compounds within 37 ppm of the theoretical mass for molecular formula with an

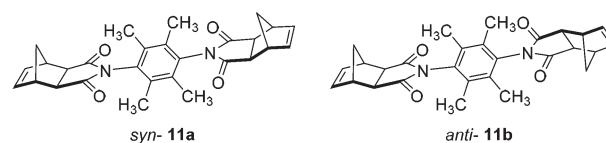


Fig. 5 *exo*-Analogues *syn*-**11a** and *anti*-**11b**.

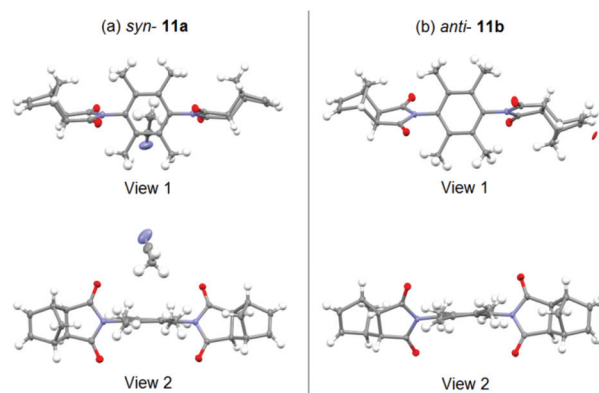


Fig. 6 X-ray crystal structures of the *exo*-analogues; (a) *syn*-**11a** (crystallised with a molecule of acetonitrile), (b) *anti*-**11b** (co-crystallised with approximately 6% mono-epoxide). Images rendered in Mercury (CCDC).<sup>91</sup>

|| Compound **10** was used due to the poor solubility of the zinc(II) metallated adduct of *exo*-porphyrin receptor **8** in chloroform.

\*\* Ref. 89 relates to anilide derivatives rather than imides, however, the principle of balancing steric and electronic factors is the same here.



additional oxygen atom (*i.e.* epoxide,  $[M + O + Na]^+$ ). There is a literature report of partial epoxide conversion of similar polycyclic derivatives during recrystallisation,<sup>92</sup> in which epoxidation is also undertaken chemically using an initiator in the presence of molecular oxygen, however it is conceivable that uninitiated epoxidation could occur at a rate too low for convenient measurement.<sup>92</sup>

### Host-guest complexations of tweezer 3 with DABCO

The interaction of the zinc(II) metallated tweezer **3** with the diamino ligand DABCO was studied independently for *syn*-**3a** and *anti*-**3b**, using UV/Vis and NMR spectroscopic titrations. Complexation models, association constants and speciation diagrams were calculated from the UV/Vis titration data similarly to other published approaches,<sup>14,17,28,95–103</sup> using HypSpec and HySS2009 (Protonic software).<sup>104,105</sup>

**syn-3a.** The *syn*-host **3a** can form various complexes with DABCO in solution, all of which are in equilibrium. These possibilities are outlined schematically in Fig. 7, and reveal the possibility of 1:1 ( $3a + DABCO \rightleftharpoons 3a \cdot DABCO$ ;  $K_{11} = [3a \cdot DABCO]/([3a][DABCO])$ ), 1:2 ( $3a + 2 \cdot DABCO \rightleftharpoons 3a \cdot (DABCO)_2$ ;  $K_{12} = [3a \cdot (DABCO)_2]/([3a][DABCO]^2)$ ), and 2:1 ( $2 \cdot 3a + DABCO \rightleftharpoons (3a)_2 \cdot DABCO$ ;  $K_{21} = [(3a)_2 \cdot DABCO]/([3a]^2[DABCO])$ ) stoichiometries.

UV/Vis titration of a solution of DABCO into a solution of *syn*-**3a** resulted in a two-stage red shift of the Soret maximum (Fig. 8), indicating the stepwise formation of two dominant complexes between *syn*-**3a** and DABCO. The first red shift, from 418.3 nm (red line) to 423.4 nm (blue line) is characteristic of a bis-porphyrin DABCO sandwich complex formation.<sup>106,107</sup> A second gradual red shift occurs to 428.6 nm (green line) by 400 000 equivalents of DABCO, although this transition appears to only be partially complete. This is characteristic of simple mono-porphyrin DABCO complexes.<sup>106,107</sup>

Fitting of the UV/Vis titration data using HypSpec<sup>104,105</sup> resulted in reasonable fits (visual inspection) to two different complexation models, including either the formation of  $3a \cdot DABCO$  and  $3a \cdot (DABCO)_2$  or the formation of  $(3a)_2 \cdot (DABCO)_2$  and  $3a \cdot (DABCO)_2$  (Fig. 7).

Fitting of an algorithm (Fig. 9 using the HypSpec protocol<sup>104,105</sup>) for the formation of the 1:1 complex  $3a \cdot DABCO$  and

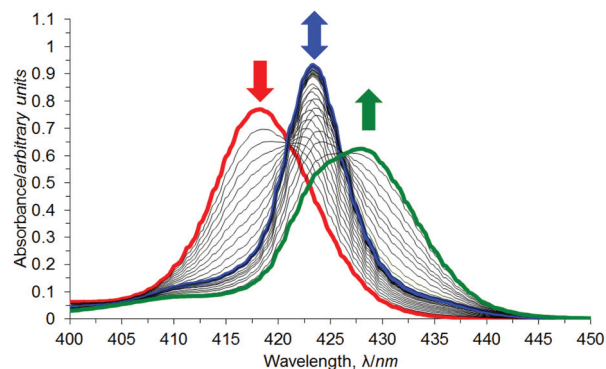


Fig. 8 UV/Vis titration of *syn*-**3a** (red line) with DABCO in chloroform.

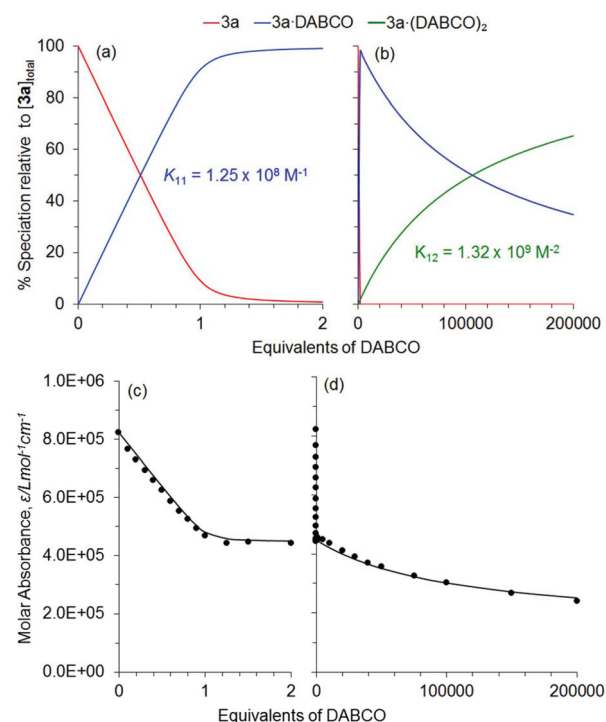


Fig. 9 Derived speciation plots (a) and (b) for formation of  $3a \cdot DABCO$  (blue line) and  $3a \cdot (DABCO)_2$  (green line) in the 0–2 equivalent and 0–200 000 equivalent ranges of added DABCO, respectively, in  $CHCl_3$  at 20 °C. The corresponding best fits, (c) and (d), of an algorithm for the formation of the 1:1 complex  $3a \cdot DABCO$  and the 1:2 complex  $3a \cdot (DABCO)_2$  (black lines) for the UV/Vis absorbance data obtained at 419 nm (black circles).

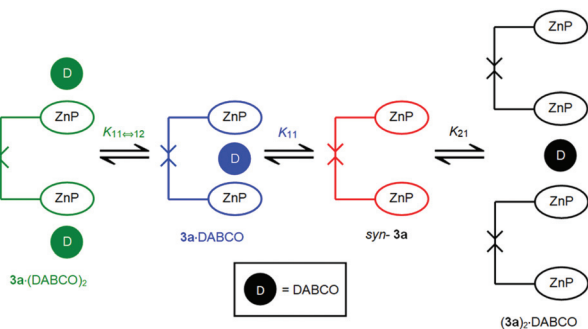


Fig. 7 Schematic representation of the various equilibria between *syn*-**3a** and DABCO.

the 1:2 complex  $3a \cdot (DABCO)_2$  (Fig. 7) to absorbance data at 419 nm obtained over a range of 200 000 equivalents of added DABCO yielded  $K_{11} = 1.25 \times 10^8 \text{ M}^{-1}$  and  $K_{12} = 1.32 \times 10^9 \text{ M}^{-2}$  in  $CHCl_3$  at 20 °C. This corresponds to a stepwise  $K'_{12} = 10.6 \text{ M}^{-1}$  for the complexation of DABCO by  $3a \cdot DABCO$  to give  $3a \cdot (DABCO)_2$ . The derived speciations for the complexation in the 0–2 and 0–200 000 equivalents of added DABCO ranges are shown in Fig. 9(a) and (b), and the corresponding data fits at 419 nm are shown in Fig. 9(c) and (d), respectively. Similar

data fits were obtained at 423 and 430 nm (not shown). The  $K_{11} = 1.25 \times 10^8 \text{ M}^{-1}$  characterising **3a**-DABCO is much larger than  $K_{11} = 2.53 \times 10^5 \text{ M}^{-1}$  (not statistically corrected) for mono-porphyrin-quinuclidine,<sup>15</sup> and is consistent with **3a**-DABCO involving bis-porphyrin complexation in the sandwich structure shown in Fig. 7.<sup>13,17,18</sup>

The UV/Vis titration data for *syn*-**3a**/DABCO could also be fitted to a complexation model involving the formation of  $(\mathbf{3a})_2:(\text{DABCO})_2$  ( $K_{22} = 1.29 \times 10^{22} \text{ M}^{-3}$ ) and  $\mathbf{3a}:(\text{DABCO})_2$  ( $K_{12} = 1.90 \times 10^9 \text{ M}^{-2}$ ) (S23†). However, the geometric constraints imposed by restricted phenyl core rotation in *syn*-**3a** limits the opportunity to form bis-porphyrin interactions with DABCO in  $(\mathbf{3a})_2:(\text{DABCO})_2$ .

The  $K_{11} = 1.25 \times 10^8 \text{ M}^{-1}$  characterising *syn*-**3a**-DABCO is approximately double that determined for freely rotating **1**-DABCO ( $K_{11} = 8.1 \times 10^7 \text{ M}^{-1}$ ).<sup>15</sup> This fits with the arc through which the two porphyrin moieties are able to move; 360° in **1** and 180° for *syn*-**3a**. This equates to *syn*-**3a** being approximately twice as pre-organised as freely rotating **1**, and which is reflected in a nearly doubling of  $K_{11}$ .

An assessment of the validity of the complexation model derived from the UV/Vis titration (carried out at micromolar concentration) may be made by using the derived complexation constants to predict the behaviour of the system during a <sup>1</sup>H NMR titration (carried out at millimolar concentration).<sup>59,106–108</sup> Thus, <sup>1</sup>H NMR titrations of *syn*-**3a**/DABCO were undertaken in CDCl<sub>3</sub>.

The resonances of sandwich *syn*-**3a** porphyrin β-pyrrole and sandwich DABCO are diagnostic in the interpretation of the complexation occurring during <sup>1</sup>H NMR titrations. At 20 °C, the β-pyrrole signals for free *syn*-**3a** occur at 8.92–8.75 ppm (Fig. 10(a)). The addition of up to 0.9 equivalents of DABCO (integration suggests 1 equivalent)†† results in the appearance of a second *syn*-**3a** β-pyrrole signal at 8.55 ppm. This upfield shift is typical of β-pyrrole protons in a bis-porphyrin DABCO sandwich complex as a consequence of shielding by opposing ring currents of two porphyrin aromatic systems in close proximity.<sup>96,106,107</sup> The two *syn*-**3a** species are in slow exchange on the NMR chemical shift timescale, and the *syn*-**3a** complex resonance intensity increases as that of free *syn*-**3a** decreases. The relative integration of the *syn*-**3a** complex β-pyrrole resonance to that of the total *syn*-**3a** β-pyrrole resonance (free plus complex) is consistent with the formation of a 1 : 1 complex (within 10% error), such as **3a**-DABCO or  $(\mathbf{3a})_2:(\text{DABCO})_2$ , and is later shown to be the former. Addition of greater than 1 equivalent of DABCO causes the *syn*-**3a** β-pyrrole resonance to shift downfield as increasing proportions of the  $\mathbf{3a}:(\text{DABCO})_2$  complex forms in fast exchange with **3a**-DABCO on the NMR chemical shift timescale. However, the change in chemical shift of this *syn*-**3a** resonance after the addition of 5 equivalents of DABCO ( $\Delta\delta = 0.033 \text{ ppm}$ ) is small compared to that of the freely rotating tweezer **1** ( $\Delta\delta = 0.082 \text{ ppm}$  (ref. 90)) under

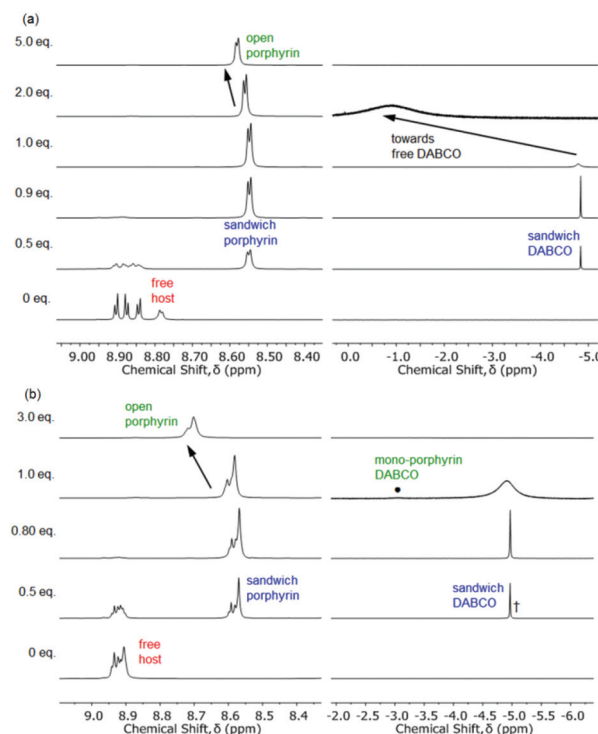


Fig. 10 Selected <sup>1</sup>H NMR spectra of *syn*-**3a** with various equivalents of DABCO at (a) 20 °C and (b) -50 °C. † identifies minor amounts of an additional sandwich complex. ● identifies the mono-porphyrin:DABCO signal broadened into the baseline due to chemical exchange. Spectra recorded at 600 MHz in CDCl<sub>3</sub>.

the same conditions, consistent with the **3a**-DABCO complex being less amenable to the addition of a second DABCO than is the **1**-DABCO complex.

The *syn*-**3a** porphyrin *meso*-phenyl proton resonances (not shown) are broadened in the presence of less than 1 equivalent of DABCO but sharpen in the presence of greater than 1 equivalent of DABCO and shift downfield, presumably as the sandwich complex forms and undergoes fast exchange with the open *syn*-**3a** complex with DABCO,  $\mathbf{3a}:(\text{DABCO})_2$ . Little information could be obtained from the polycyclic resonances.

Further understanding of the complexation of DABCO by *syn*-**3a** is gained from the DABCO methylene resonance (Fig. 10(a)). For the addition of up to 0.9 equivalents of DABCO (integration suggests 1 equivalent), a sharp singlet was observed at -4.84 ppm. This large upfield shift is typical of DABCO methylene protons in a bis-porphyrin DABCO sandwich complex, and again results from shielding by opposing ring currents of two porphyrin aromatic systems in close proximity.<sup>96,106,107,109–112</sup> The relative integration of the DABCO sandwich resonance to the *syn*-**3a** ester signal†† is con-

†† The error between the number of equivalents of DABCO titrated with tweezer **3**, based on mass weighed, compared to the NMR signal integration was estimated to be 10% at 20 °C for both *syn*-**3a** and *anti*-**3b**, 20% at -50 °C for *syn*-**3a**, and 10–15% at -50 to -60 °C for *anti*-**3b**.

†† The ester signal was selected as a reference because it does not change chemical shift significantly on complexation, and its integration is the sum of free plus complexed species. Conveniently, the number of protons in the host ester resonance is equal to the number of protons in an isolated molecule of free DABCO, and so their relative integrations do not require any normalisation.





sistent with the formation of a species with the empirical formula of 1 : 1 (within 10% error). At 1 equivalent and greater of DABCO, the sandwich DABCO resonance broadens, and migrates downfield towards the value for free DABCO. This is consistent with chemical exchange with another species occurring at a fast exchange rate on the NMR chemical shift timescale at 20 °C, most likely a combination of  $3a \cdot (DABCO)_2$  and free DABCO.

At less than 1 equivalent of DABCO, all resonances, including the *syn*- $3a$  porphyrin and polycyclic resonances, are in slow exchange on the NMR chemical shift timescale, however, several of the free *syn*- $3a$  host resonances undergo simultaneous resonance shifts as their signal intensity is depleted and the complex resonance increases (not shown). This was particularly obvious for the methylene bridgehead proton at 1.0–1.3 ppm and the porphyrin  $\beta$ -pyrrole resonance. This phenomenon appears to indicate a second process occurring in addition to formation of the sandwich complex. This could be attributed to the concentration dependence of the free host  $^1H$  NMR spectrum discussed earlier (S12(a)†). In this case, as the *syn*- $3a$  complex forms, the free *syn*- $3a$  concentration decreases and its concentration dependent chemical shift changes.

Slowing the exchange rate between the various *syn*- $3a$  complexes in solution was achieved by lowering the sample temperature to  $-50$  °C (Fig. 10(b)), and revealed several additional spectral features. Below 0.8 equivalents of DABCO (integration suggests 1 equivalent), a small amount of an additional sandwich *syn*- $3a$  complex in addition to the main signal can be observed around  $-5$  ppm (indicated by † in Fig. 10(b)). At greater than 0.8 equivalents of DABCO (spectral features suggest greater than 1 equivalent), the system moves into fast exchange on the NMR chemical shift timescale. A small amount of the open *syn*- $3a$  complex can be observed at  $-3.06$  ppm (indicated by ● in Fig. 10(b)) in addition to the main sandwich *syn*- $3a$  complex resonance, now broadened due to chemical exchange. The resonance at  $-3.06$  ppm is characteristic of the  $\alpha$  methylene protons of DABCO bound to a single porphyrin,<sup>106,108,111</sup> and most likely corresponds to conversion of the sandwich *syn*- $3a$  complex to open species, in this case  $3a \cdot (DABCO)_2$ .

The porphyrin *meso*-phenyl protons (not shown) are sharp and highly desymmetrised below 1 equivalent of DABCO, indicating facial differentiation of the porphyrins within the sandwich complex. For greater than 1 equivalent of DABCO, the porphyrin *meso*-phenyl protons broaden and resymmetrise, suggesting diminishing facial discrimination, then shift downfield, presumably as the sandwich complex undergoes fast exchange with open species on the NMR chemical shift timescale. Little information could be obtained from the polycyclic resonances.

To further investigate the composition of the complex formed between *syn*- $3a$  and DABCO at NMR concentrations (millimolar), a simulated NMR speciation diagram was generated in HySS2009<sup>104,105</sup> using the association constants for successfully fitted complexation models determined from the

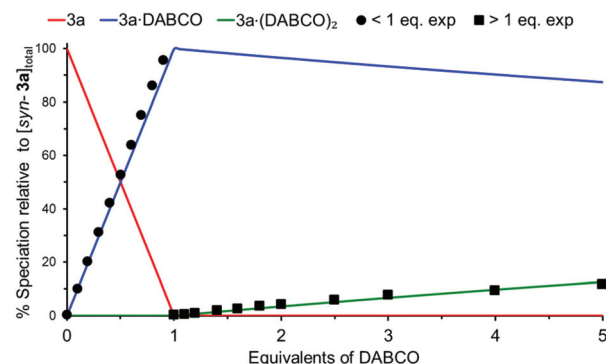


Fig. 11 Simulated NMR speciation diagram (millimolar) generated from UV/Vis determined association constants  $K_{11}$  and  $K_{12}$  for *syn*- $3a$ /DABCO (micromolar). Experimental NMR speciation has been overlayed for both the slow and fast exchange regions of the titration.

UV/Vis titrations (micromolar), and compared with experimental NMR titration data.<sup>106–108</sup> Fig. 11 shows this result for the 1 : 1 plus 1 : 2 complexation model, where the blue line represents the predicted NMR speciation for the growth and decay of  $3a \cdot DABCO$ , the green line represents the open species  $3a \cdot (DABCO)_2$ , and the red line represents free host. The black circles and squares represent the experimental speciation for the slow and fast exchange NMR chemical shift timescale regions respectively, calculated as described in S22.† §§

As can be seen in Fig. 11, there is excellent agreement between the simulated and experimental speciation across both the slow and fast exchange NMR chemical shift timescale regions. This confirmed that the complexation model was the same at both UV/Vis and NMR concentrations for the *syn*- $3a$ /DABCO system; formation of the sandwich complex  $3a \cdot DABCO$  and gradual decay of the sandwich complex into open complex  $3a \cdot (DABCO)_2$ . The simulated NMR speciation for the alternative complexation model from the UV/Vis data involving the formation of  $(3a)_2 \cdot (DABCO)_2$  and  $3a \cdot (DABCO)_2$  is shown in S23,† however, does not match the experimental data for the formation of the open species  $3a \cdot (DABCO)_2$ .

**anti-3b.** On the other hand, the geometric constraints imposed by the restricted rotation of the phenyl core enable the *anti*-conformation to form different complexes to the *syn*-conformation. The *anti*- $3b$  host can form various complexes with DABCO in solution, all of which are in equilibrium. These possibilities are outlined schematically in Fig. 12, and reveal the possibility of 2 : 2 ( $2 \cdot 3b + 2 \cdot DABCO \rightleftharpoons (3b)_2 \cdot (DABCO)_2$ ;  $K_{22} = [(3b)_2 \cdot (DABCO)_2] / ([3b]^2 [DABCO]^2)$ ), 1 : 2 ( $3b + 2 \cdot DABCO \rightleftharpoons 3b \cdot (DABCO)_2$ ;  $K_{12} = [3b \cdot (DABCO)_2] / ([3b] [DABCO]^2)$ ), 2 : 1 ( $2 \cdot 3b + DABCO \rightleftharpoons (3b)_2 \cdot DABCO$ ;  $K_{21} = [(3b)_2 \cdot DABCO] / ([3b]^2 [DABCO])$ ) stoichiometries, as well as a  $n:n$  polymeric assembly ( $n \cdot 3b + n \cdot DABCO \rightleftharpoons (3b)_n \cdot (DABCO)_n$ ;  $K_{nn} = [(3b)_n \cdot (DABCO)_n] / ([3b]^n [DABCO]^n)$ ).

§§ A chemical shift of 8.548 ppm (*syn*- $3a$  + 0.9 eq. DABCO) was selected for the value for fully complexed species. A chemical shift of 8.829 ppm (*anti*- $3b$  + 5 eq. DABCO) was selected for the value for fully open species.





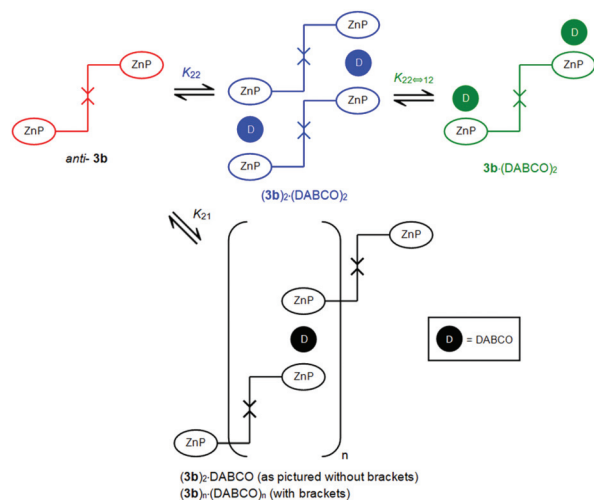


Fig. 12 Schematic representation of the various equilibria between *anti*-**3b** and DABCO.

UV/Vis titration of a solution of DABCO into a solution of *anti*-**3b** again resulted in a two-stage redshift of the Soret maximum (Fig. 13), indicating the stepwise formation of two dominant complexes between *anti*-**3b** and DABCO. The first red shift, from 419.5 nm (red line) to 423.5 nm (blue line) is characteristic of a bis-porphyrin DABCO sandwich complex formation.<sup>106,107</sup> However, this sandwich species is transient, and a second redshift occurs to 430.0 nm (green line) by 10 000 equivalents of DABCO, after which this transition appears to be complete. This is characteristic of simple monoporphyrin DABCO complexes.<sup>106,107</sup>

Fitting of the UV/Vis titration data using HypSpec<sup>104,105</sup> resulted in reasonable fits (visual inspection) to several different complexation models, including the formation of  $(3b)_2 \cdot (DABCO)_2$  and  $3b \cdot (DABCO)_2$ , and the formation of  $3b \cdot DABCO$  and  $3b \cdot (DABCO)_2$  (Fig. 12).

Fitting of an algorithm (Fig. 14 using the HypSpec protocol<sup>104,105</sup>) for the formation of the 2:2 complex  $(3b)_2 \cdot (DABCO)_2$  and the 1:2 complex  $3b \cdot (DABCO)_2$  (Fig. 12) to absorbance data at 419 nm obtained over a range of 10 000

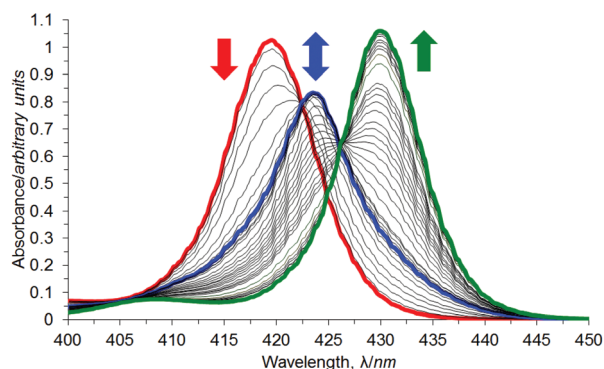


Fig. 13 UV/Vis titration of *anti*-**3b** (red line) with DABCO in chloroform.

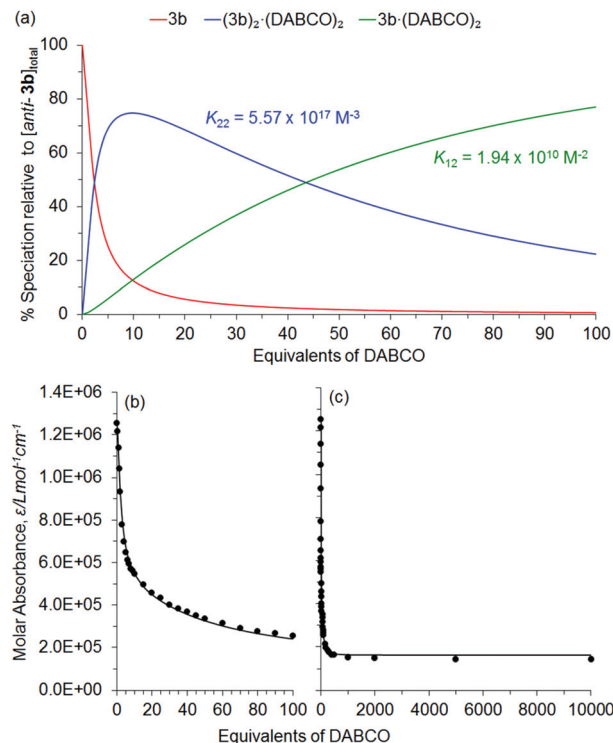


Fig. 14 Derived speciation plot (a) for formation of  $(3b)_2 \cdot (DABCO)_2$  (blue line) and  $3b \cdot (DABCO)_2$  (green line) for 0–10 000 equivalents of added DABCO in  $CHCl_3$  at 20 °C. The corresponding best fits, (c) and (d), of an algorithm for the formation of the 2:2 complex  $(3b)_2 \cdot (DABCO)_2$  and the 1:2 complex  $3b \cdot (DABCO)_2$  (black lines) for the UV/Vis absorbance data obtained at 419 nm (black circles) for 0–100 and 0–10 000 equivalents of added DABCO respectively.

equivalents of added DABCO yielded  $K_{22} = 5.57 \times 10^{17} \text{ M}^{-3}$  and  $K_{12} = 1.94 \times 10^{10} \text{ M}^{-2}$  in  $CHCl_3$  at 20 °C. The value for  $K_{22}$  compares well to other similar porphyrin-DABCO sandwich complexes in the literature ( $K_{22} = 6.2 \times 10^{16}$ – $6.3 \times 10^{22} \text{ M}^{-3}$ ).<sup>106–108</sup> The derived speciation for the complexation with 0–10 000 equivalents of added DABCO is shown in Fig. 14(a), and the corresponding data fit at 419 nm is shown in Fig. 14(b) and (c), for 0–100 and 0–10 000 equivalents of added DABCO respectively. Similar data fits were obtained at 423 and 430 nm (not shown).

The UV/Vis titration data for *anti*-**3b**/DABCO could also be fitted to a complexation model involving the formation of  $3b \cdot DABCO$  ( $K_{11} = 7.16 \times 10^5 \text{ M}^{-1}$ ) and  $3b \cdot (DABCO)_2$  ( $K_{12} = 2.17 \times 10^{10} \text{ M}^{-2}$ ) (S24†). However, the goodness of the fit alone cannot be used as the criterion to decide the correct complexation model,<sup>106</sup> and all aspects of the fitting output should be examined (S22†). In this case, the calculated UV/Vis spectra in the HypSpec output (not shown) suggested the  $3b \cdot DABCO$  species had a wavelength maxima centred around 423 nm, which would experimentally suggest a bis-porphyrin DABCO sandwich complex. However, the geometric constraints imposed by restricted phenyl core rotation in *anti*-**3b** limit the opportunity to form bis-porphyrin interactions with DABCO in  $3b \cdot DABCO$ , and so this complexation model was excluded.



Subsequently,  $^1\text{H}$  NMR titrations of *anti-3b*/DABCO were undertaken in  $\text{CDCl}_3$ . At 20 °C, the  $\beta$ -pyrrole signals for free *anti-3b* occur at 8.96–8.94 ppm (Fig. 15(a)). The addition of up to 0.9 equivalents of DABCO (integration suggests 1 equivalent) $\dagger\dagger$  results in the appearance of a second *anti-3b*  $\beta$ -pyrrole signal for the complex at 8.55 ppm. The two *anti-3b* species are in slow to medium exchange on the NMR chemical shift timescale (resonances are broad but distinct) and the *anti-3b* complex resonance intensity increases as that of free *anti-3b* decreases. The relative integration of the *anti-3b* complex  $\beta$ -pyrrole resonance to that of the total *anti-3b*  $\beta$ -pyrrole resonance (free plus complex) is consistent with the formation of a species with the empirical formula of 1 : 1 (within 10% error), such as  $(\mathbf{3b})_2\cdot(\text{DABCO})_2$  or  $(\mathbf{3b})_n\cdot(\text{DABCO})_n$ . This chemical shift of this complex resonance (8.55 ppm) is typical of  $\beta$ -pyrrole protons in a bis-porphyrin DABCO sandwich,<sup>96,106,107</sup> and so a complexation model involving  $\mathbf{3b}$ -DABCO can again be excluded due to geometric constraints as previously discussed. Addition of greater than 1 equivalent of DABCO causes the *anti-3b*  $\beta$ -pyrrole resonance to shift downfield as increasing proportions of  $\mathbf{3b}\cdot(\text{DABCO})_2$  forms in fast exchange with  $(\mathbf{3b})_2\cdot(\text{DABCO})_2$  on the NMR chemical shift timescale. However, the change in chemical shift of this *anti-3b* resonance after the addition of 5 equivalents of DABCO ( $\Delta\delta =$

0.282 ppm) is larger than for the freely rotating **1** and *syn-3a* tweezer systems ( $\Delta\delta = 0.082$  (ref. 90) and 0.033 ppm respectively) under the same conditions. This demonstrates the increased formation of  $\mathbf{3b}\cdot(\text{DABCO})_2$  from  $(\mathbf{3b})_2\cdot(\text{DABCO})_2$  for excess DABCO, compared to **1** $\cdot(\text{DABCO})_2$  from **1**-DABCO, and **3a** $\cdot(\text{DABCO})_2$  from **3a**-DABCO.

The *anti-3b* porphyrin  $\beta$ -pyrrole (shown) and *meso*-phenyl signals (not shown) are broadened in the presence of less than 5 equivalents of DABCO, at which point they sharpen after the shift downfield, presumably as  $(\mathbf{3b})_2\cdot(\text{DABCO})_2$  undergoes fast exchange with increasing proportions of  $\mathbf{3b}\cdot(\text{DABCO})_2$ . Little information could be obtained from the polycyclic resonances.

Further understanding of the complexation of DABCO by *anti-3b* is gained from the DABCO methylene resonance (Fig. 15(a)). At 0.1 equivalents of DABCO (not shown), two signals can be observed; major at  $-4.826$  ppm and minor at  $-4.846$  ppm. This large upfield shift is typical of DABCO methylene protons in a bis-porphyrin DABCO sandwich complex,<sup>96,106,107,109–112</sup> and indicates the formation of two different sandwich complexes. At 0.5 equivalents of DABCO, only the major signal can be observed, and is a sharp singlet for up to 0.9 equivalents of DABCO (integration suggests 1 equivalent). The relative integration of the DABCO sandwich resonance to the *anti-3b* ester signal $\ddagger\ddagger$  is consistent with the formation of a species with the empirical formula of 1 : 1 (within 10–15% error), such as  $(\mathbf{3b})_2\cdot(\text{DABCO})_2$  or  $(\mathbf{3b})_n\cdot(\text{DABCO})_n$ . At 1 equivalent and greater of DABCO, the sandwich DABCO resonance broadens. This is consistent with chemical exchange with another species occurring at a fast exchange rate on the NMR chemical shift timescale at 20 °C, most likely a combination of  $\mathbf{3b}\cdot(\text{DABCO})_2$  and free DABCO. At 5 equivalents of DABCO, a broad signal was observed between 0.8–2.2 ppm under the polycyclic signals (not shown), shifting towards the resonance for free DABCO.

Slowing the exchange rate between the various *anti-3b* complexes in solution was achieved by lowering the sample temperature to  $-50$  and  $-60$  °C (Fig. 15(b)), and revealed several additional spectral features. Below 0.9 equivalents of DABCO (integration suggests 1 equivalent), two sandwich *anti-3b* complexes can be identified from the DABCO signals at  $-4.89$  ppm and  $-4.90$  ppm. The species at  $-4.90$  ppm is dominant below 0.3 equivalents of DABCO after which the species at  $-4.89$  ppm becomes dominant. A trace quantity of a third sandwich complex was observed at  $-4.98$  ppm. These sandwich species are marked  $\dagger$  in Fig. 15(b). Additional evidence for two sandwich *anti-3b* complexes at low temperature was observed in several of the polycyclic resonances (not shown), several of which are split into three; free *anti-3b* and two complexes. These are most likely to be different molecular orientations of  $(\mathbf{3b})_2\cdot(\text{DABCO})_2$  (see molecular modelling section), or  $(\mathbf{3b})_n\cdot(\text{DABCO})_n$ . At greater than 1 equivalent of DABCO, the system remained in slow to intermediate exchange on the NMR chemical shift timescale, and allowed the resonances for the open *anti-3b*/DABCO complex,  $\mathbf{3b}\cdot(\text{DABCO})_2$ , to be assigned. The open porphyrin  $\beta$ -pyrrole resonance for  $\mathbf{3b}\cdot(\text{DABCO})_2$  occurs at 8.88 ppm, while the DABCO

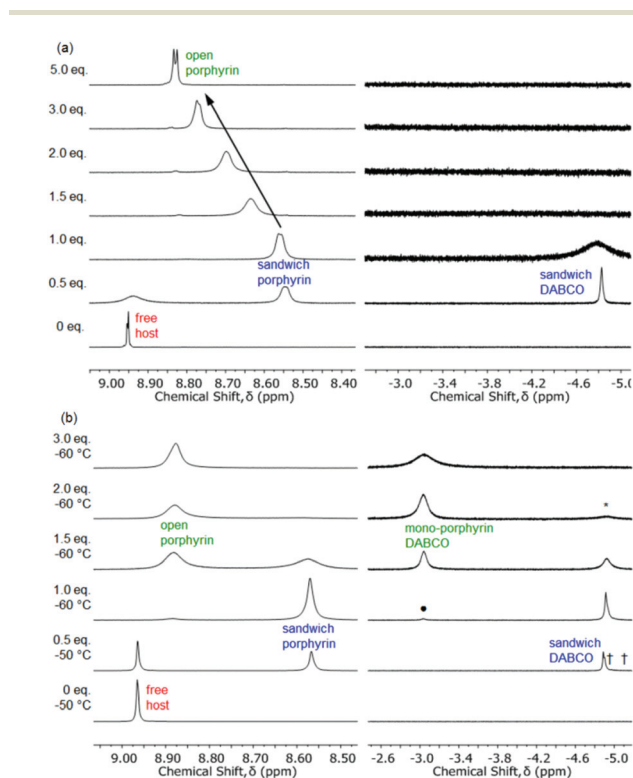


**Fig. 15** Selected  $^1\text{H}$  NMR spectra of *anti-3b* with various equivalents of DABCO at (a) 20 °C and (b)  $-50$  to  $-60$  °C.  $\dagger$  identifies additional sandwich complexes.  $*$  identifies DABCO sandwich signals broadened into the baseline due to chemical exchange.  $\bullet$  identifies the mono-porphyrin-DABCO signal broadened into the baseline due to chemical exchange. Spectra recorded at 600 MHz in  $\text{CDCl}_3$ .



$\alpha$ -methylene resonance in  $3b \cdot (DABCO)_2$  occurs at  $-3.04$  ppm (marked ● in Fig. 15(b)). Both of these chemical shifts are consistent with DABCO interacting with a mono-porphyrin.<sup>106,108,111</sup> These resonances increase in intensity at the expense of those for the sandwich *anti*- $3b$  complex,  $(3b)_2 \cdot (DABCO)_2$ , with the conversion to  $3b \cdot (DABCO)_2$  almost complete at 2 equivalents of DABCO. This again demonstrates the increased formation of  $3b \cdot (DABCO)_2$  from  $(3b)_2 \cdot (DABCO)_2$  for excess DABCO, compared to  $1 \cdot (DABCO)_2$  from  $1 \cdot DABCO$ , and  $3a \cdot (DABCO)_2$  from  $3a \cdot DABCO$ . At 3 equivalents of DABCO, the mono-porphyrin DABCO resonance for  $3b \cdot (DABCO)_2$  broadens, presumably due to exchange with free DABCO.

Interestingly, there is a broad signal at a chemical shift of  $0.82$  ppm (not shown) at  $-50^\circ\text{C}$ , which increases in intensity between 1–2 equivalents of DABCO. This was tentatively assigned to the  $\beta$ -methylene of DABCO interacting with a mono-porphyrin, such as  $3b \cdot (DABCO)_2$ , in the absence of a literature value (quinuclidine  $\beta$ -methylene protons occur at  $-0.64$  ppm for their complex with mono-porphyrins<sup>111</sup>).

To further investigate the composition of the complex formed between *anti*- $3b$  and DABCO at NMR concentrations (millimolar), a simulated NMR speciation diagram was generated in HySS2009<sup>104,105</sup> using the association constants for successfully fitted complexation models determined from the UV/Vis titrations (micromolar), and compared with experimental NMR titration data.<sup>106–108</sup> Fig. 16 shows this result for the 2 : 2 plus 1 : 2 complexation model, where the blue line represents the predicted NMR speciation for the growth and decay of  $(3b)_2 \cdot (DABCO)_2$ , the green line represents the open species  $3b \cdot (DABCO)_2$ , and the red line represents free host. The black circles and squares represent the experimental speciation for the slow and fast exchange NMR chemical shift timescale regions respectively, calculated as described in S22.†<sup>†</sup>

As can be seen in Fig. 16, there is excellent agreement between the simulated and experimental speciation in the slow exchange NMR chemical shift timescale region ( $<1$  eq. DABCO), while the simulation follows the same trend as the experimental data in the fast exchange NMR chemical shift timescale region ( $>1$  eq. DABCO). This confirmed that the complexation model was the same at both UV/Vis and NMR concentrations for the *anti*- $3b$ /DABCO system; formation of the sandwich complex  $(3b)_2 \cdot (DABCO)_2$  and decay of the sandwich complex into open complex  $3b \cdot (DABCO)_2$  (assuming that the major and minor sandwich species observed in the NMR at low equivalents of DABCO are two different molecular orientations of  $(3b)_2 \cdot (DABCO)_2$ , and not  $(3b)_n \cdot (DABCO)_n$ ). The simulated NMR speciation for the alternative complexation model,  $3b \cdot DABCO$  and  $3b \cdot (DABCO)_2$ , excluded during the analysis of both the UV/Vis and NMR data, is shown in S24,† however, does not match the experimental data for the formation of either  $3b \cdot DABCO$  or  $3b \cdot (DABCO)_2$ .

†† The major and minor signals for the sandwich species observed at low equivalents of DABCO were not baseline resolved and so were integrated together, which assumes that the two resonances arise from different molecular orientations of the same complex  $(3b)_2 \cdot (DABCO)_2$ .

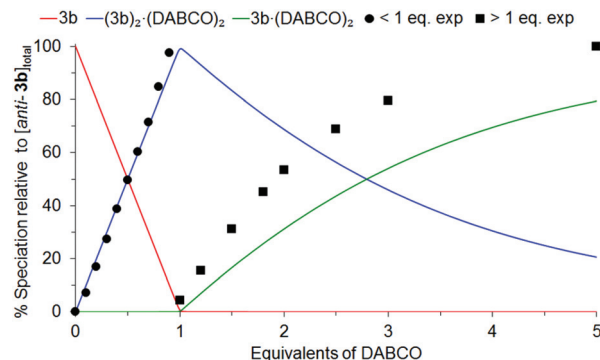


Fig. 16 Simulated NMR speciation diagram (millimolar) generated from UV/Vis determined association constants  $K_{22}$  and  $K_{12}$  for *anti*- $3b$ /DABCO (micromolar). Experimental NMR speciation has been overlayed for both the slow and fast exchange regions of the titration.

### Molecular modelling

Molecular modelling<sup>93</sup> was undertaken to provide information on the equilibrium geometry of the restricted rotation tweezer in the absence of guest (semi-empirical, AM1), and is shown in Fig. 17. For the *syn*- $3a$  conformation, rotation of the polycyclic arms can be observed about the central 2,3,5,6-tetramethylphenyl diimide group. Although the bis-porphyrins in the free host are not arranged in a cofacial orientation in the model, rotation about porphyrin *meso*-phenyl groups is well known,<sup>113–115</sup> and this would enable the formation of the sandwich *syn*- $3a$ ·DABCO complex that is observed experimentally. For the *anti*- $3b$  conformation, it is evident from the model that a sandwich *anti*- $3b$ ·DABCO complex cannot be accessed due to geometry constraints in the free host, but that the sandwich *anti*-( $3b$ )<sub>2</sub>·(DABCO)<sub>2</sub> complex that was observed experimentally is supported by the model.

Finally, molecular modelling (semi-empirical, AM1)<sup>93</sup> was undertaken to determine the equilibrium geometry of DABCO complexes of *syn*- $3a$  and *anti*- $3b$  (Fig. 18 and 19). The model of the *syn*- $3a$ ·DABCO complex (Fig. 18) appears similarly to our previously described freely rotating tweezer  $1 \cdot DABCO$ .<sup>15</sup> Rotation is observed about the porphyrin moieties as well as between the two polycyclic arms of the tweezer about the central 2,3,5,6-tetramethylphenyl diimide group. The core is

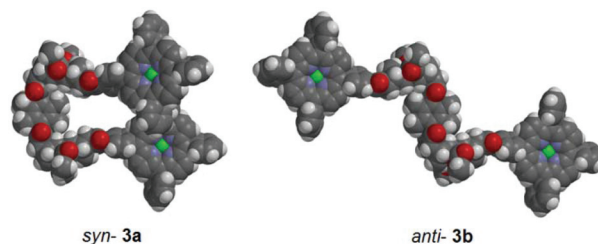


Fig. 17 Equilibrium geometry of *syn*- $3a$  and *anti*- $3b$  in the absence of guest (semi-empirical, AM1).





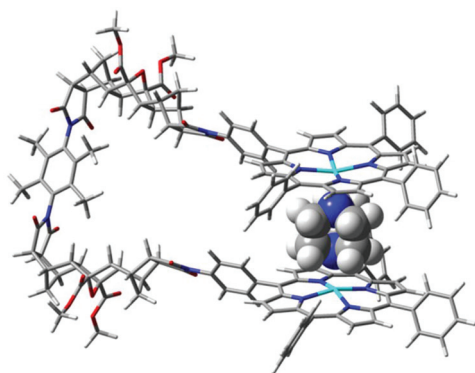


Fig. 18 Equilibrium geometry (semi-empirical, AM1) of *syn*-**3a**-DABCO. Image rendered in GaussView.<sup>116</sup>

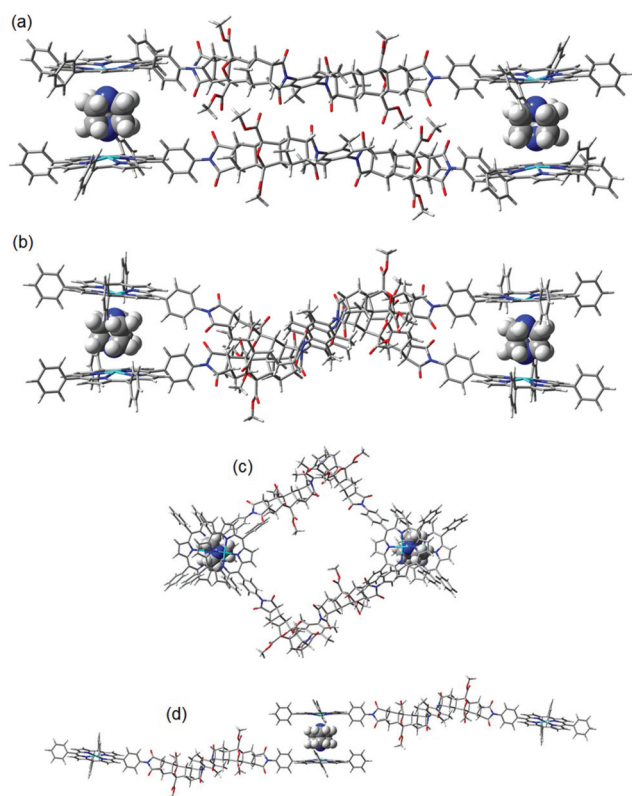


Fig. 19 Equilibrium geometry (semi-empirical, AM1) of (a)–(c) different orientations of *anti*-(**3b**)<sub>2</sub>·(DABCO)<sub>2</sub>; (d) *n*:*n* polymeric assembly *anti*-(**3b**)<sub>*n*</sub>·(DABCO)<sub>*n*</sub> (truncated). Image rendered in GaussView.<sup>116</sup>

partially distorted from planarity,<sup>|||</sup> as was observed experimentally in the X-ray crystallographic structures of related compound **11** (Fig. 6). Overlay of the polycyclic arms in models with and without DABCO (not shown) revealed only minimal

<sup>|||</sup> While the 2,3,5,6-tetramethylphenyl diimide group is distorted from planarity, no curvature was observed along the norbornyl diimide plane. A degree of curvature was observed in the analogous model of the freely rotating tweezer with guest, **1**-DABCO.<sup>90</sup>

distortion, providing further evidence that the polycyclic arms are essentially rigid. The overall complexed structure does not appear to be significantly strained, and this supports the high association constant that has been determined experimentally.

The *anti*-(**3b**)<sub>2</sub>·(DABCO)<sub>2</sub> complex could exist in several molecular orientations, for example where the polycyclic linkers are stacked horizontally, vertically, or adopt a four sided structure (Fig. 19(a)–(c) respectively). In addition, the *n*:*n* polymeric assembly, *anti*-(**3b**)<sub>*n*</sub>·(DABCO)<sub>*n*</sub>, is shown in Fig. 19(d), truncated to show a single repeating unit. No further investigation has been conducted into the identity of the several sandwich species observed during the NMR titration of *anti*-**3b** with DABCO.

## Conclusions

The degree of rotation in our tweezer architecture was restricted from freely rotating by fully substituting the phenyl diimide linker core with methyl groups. Evidence of restricted rotation preventing interconversion between the *syn*- and *anti*-conformations was provided by UV/Vis and NMR spectroscopy, host-guest complexation models and speciation, and X-ray crystallography.

UV/Vis and NMR titration confirmed that complexation between *syn*-**3a** and DABCO is best described by a **3a**·DABCO and **3a**·(DABCO)<sub>2</sub> complexation model. The large association constant obtained for *syn*-**3a**·DABCO ( $K_{11} = 1.25 \times 10^8 \text{ M}^{-1}$ ) indicates the tweezer is sufficiently preorganised for DABCO. This is a similar outcome to freely rotating **1**-DABCO ( $K_{11} = 8.1 \times 10^7 \text{ M}^{-1}$  (ref. 15)), which is also sufficiently preorganised for DABCO. The microscopic effective molarity,<sup>117–119</sup> EM (divided by the statistical factor,  $K_{\sigma}$ ), was calculated to be  $9.76 \times 10^{-4} \text{ M}$  for *syn*-**3a**·DABCO ( $K_{\sigma} = 8$ ),  $6.33 \times 10^{-4} \text{ M}$  for freely rotating **1**-DABCO ( $K_{\sigma} = 8$ ), and  $1.70 \times 10^{-5} \text{ M}$  for *anti*-(**3b**)<sub>2</sub>·(DABCO)<sub>2</sub> ( $K_{\sigma} = 128$ ) (S25†). Effective molarity values of other porphyrin host-guest systems in the literature usually range between  $10^{-3}$ – $10^1 \text{ M}$ ,<sup>10,59,106,107,109,118 \*\*\*</sup> although larger values have been reported.<sup>11,119</sup> Further work is underway in our laboratory to examine the difference in preorganisation between *syn*-**3a** and freely rotating **1**, which is expected to be manifested for ligands with length much greater than DABCO (2.64 Å) where the required interporphyrin distance for guest complexation requires significant rotation through the phenyl diimide linker core. Molecular modelling of *syn*-**3a**·DABCO suggests that the interporphyrin distance is modulated by partial rotation of the polycyclic scaffold about the 2,3,5,6-tetramethylphenyl diimide core, with the polycyclic scaffold remaining rigid. Nevertheless, the combined results of both this manuscript

\*\*\* Effective molarity is sometimes reported as the microscopic effective molarity multiplied by the statistical factor,  $K_{\sigma}$ .<sup>117–119</sup> Our  $K_{\sigma}$ -EM values are  $7.81 \times 10^{-3} \text{ M}$  for *syn*-**3a**·DABCO,  $5.06 \times 10^{-3} \text{ M}$  for freely rotating **1**-DABCO, and  $2.18 \times 10^{-3} \text{ M}$  for *anti*-(**3b**)<sub>2</sub>·(DABCO)<sub>2</sub>. Additionally, the determination of  $K_{\sigma}$  sometimes varies,<sup>128</sup> which can influence the statistically corrected microscopic effective molarity.





and our previous work<sup>15</sup> are in agreement with the concept that the linker need only confer the system with moderate or sufficient preorganisation to obtain a large association constant that is enhanced compared to the reference monomeric complex.<sup>§</sup>

As expected, the UV/Vis and NMR titrations of *anti*-**3b** with DABCO confirmed its non-tweezer like behaviour compared to *syn*-**3a**, and was best described by a  $(\mathbf{3b})_2(\text{DABCO})_2$  and  $\mathbf{3b}(\text{DABCO})_2$  complexation model. The NMR data indicated the formation of major and minor sandwich species, most likely different orientations of *anti*-( $\mathbf{3b})_2(\text{DABCO})_2$ , or *n:n* polymeric *anti*-( $\mathbf{3b})_n(\text{DABCO})_n$ , as represented by molecular modelling.

## Experimental

### Molecular modelling

Molecular modelling was undertaken using the Wavefunction Spartan '10 software package.<sup>93</sup> Equilibrium geometry energy minimisation was calculated using a semi-empirical AM1 model.

### Characterisation

Melting points were measured using a Barloworld Scientific SMP10 melting point apparatus. Theoretical mass spectra were generated by using the mMass software package.<sup>120</sup>

NMR spectra were recorded on a Bruker UltraShield Avance III 600 MHz NMR Spectrometer running the TopSpin software package at 293 K (20 °C). Spectra were calibrated to the residual solvent signal.<sup>121</sup>  $\text{CDCl}_3$  was deacidified by passing through neutral activated aluminium oxide (Scharlau, activity degree 1, 70–290 mesh, grain size 0.05–0.2 mm) and stored under a nitrogen atmosphere over silver foil/molecular sieves in a brown glass bottle.

X-ray diffraction intensity data for compounds **11a** and **11b** was collected with an Oxford Diffraction SuperNova CCD diffractometer using Cu-K $\alpha$  radiation. The temperature during data collection was maintained at 130.00(10) using an Oxford Cryosystems cooling device. The structure was solved by direct methods and difference Fourier synthesis.<sup>122</sup> Thermal ellipsoid plots were generated using the program ORTEP-3<sup>123</sup> integrated within the WINGX<sup>124</sup> suite of programs. Additional information on the crystal structures of compounds **11a** and **11b** can be found in the ESI (see S18 and S21†). CCDC 1526930–1526931† contain the supplementary crystallographic data for this paper.

UV/Vis spectra were recorded on a Cary 50 instrument at 20 °C in a Starna Type 21 SX 1 cm<sup>2</sup> quartz cuvette with the following parameters: average time 0.05 s, data interval 0.15 nm, scan rate 180 nm min<sup>-1</sup>, wavelength range 300–700 nm, baseline correction to blank solvent. Dry  $\text{CHCl}_3$  for recording spectra was prepared under a nitrogen atmosphere first by reflux over  $\text{P}_2\text{O}_5$  then distillation,<sup>125</sup> and deacidified and stored the same as above for  $\text{CDCl}_3$ .

### Reagents

Where necessary, solvents and reagents for synthesis were purified according to the methods published.<sup>125</sup> Dry THF was freshly distilled from sodium/benzophenone, dry  $\text{CH}_2\text{Cl}_2$  freshly distilled from  $\text{CaH}_2$ , and dry DMF and DMSO were distilled under reduced pressure onto fresh molecular sieves after stirring on molecular sieves overnight. The following chemicals were purified by sublimation under high vacuum at 0.17 mmHg at the following temperatures, then stored under a nitrogen atmosphere, protected from light, and in a desiccator at room temperature unless otherwise specified: potassium *tert*-butoxide at 160 °C, DABCO twice at 75 °C and stored at –20 °C. 2,3,5,6-tetramethyl-*p*-phenylenediamine **5** (Sigma-Aldrich) was used as purchased.

Silica gel (Davisil, 60 Å, 40–63  $\mu\text{m}$ , Grace Davison Discovery Sciences) was used for column chromatography. Kieselgel silica gel 60 F254 aluminium sheets (Merck) was used for TLC. Colourless compounds were visualised using a UV lamp or permanganate dip stain.

### Methodology for host–guest titrations

All samples for host–guest titrations were weighed using a five decimal point balance (Shimadzu AUW220D or AandD GR-202). Volumetric glassware (class A) was used for volumes >1 mL. Gas tight microlitre syringes (SGE, Hamilton) were used for volumes  $\leq 1$  mL. UV/Vis host–guest titrations were carried out at constant host concentrations of  $10^{-6}$ – $10^{-7}$  M in  $\text{CHCl}_3$  (absorbance of free host <1 absorbance unit). Complexation models, association constants and speciation diagrams were calculated from the UV/Vis titration data using the HypSpec and HySS2009 software packages (Protonic software)<sup>104,105</sup> over 400–450 nm. A more detailed discussion of examining the fitting can be found in S22.† <sup>1</sup>H NMR host–guest titrations were carried out in  $\text{CDCl}_3$  at non-constant host concentration, starting at  $10^{-3}$ – $10^{-4}$  M, and gradually diluted by aliquots of guest solution (usually 5–10  $\mu\text{L}$  per 0.1 equivalents of guest). Low temperature NMR was undertaken at –50 to –60 °C.

### General procedure for sealed tube ACE reactions

An 80 mL sealed tube (BSG Glassware, Tasmania, screw thread stopper with upper and lower Viton O-rings) was fitted with a stirrer bar and loaded with 0.8 g combined starting materials suspended in no more than 20 mL of solvent (less than one quarter total volume of flask). The tube was wrapped in alfoil, immersed in an oil bath relative to the solvent level, and heated to 160 °C with stirring for 24 hours behind a blast shield. O-rings (Viton) were replaced for each reaction.

### General procedure for porphyrin zinc(II) metallation

Using standard porphyrin zinc(II) metallation conditions,<sup>66</sup> a solution of  $\text{Zn}(\text{OAc})_2 \cdot 2\text{H}_2\text{O}$  (excess, usually 5–10 eq. per porphyrin) in MeOH was added dropwise down the condenser to a refluxing solution of porphyrin in  $\text{CHCl}_3$  (or  $\text{CH}_2\text{Cl}_2$ )/MeOH (approx. 4:1), such that the combined volume was  $\text{CHCl}_3 \geq \text{MeOH}$ . The solution was refluxed for 1–2 hours, with further



CHCl<sub>3</sub> added during this time as necessary to prevent evaporation to dryness or precipitation of the porphyrin. The mixture was cooled, diluted with CHCl<sub>3</sub>, washed with H<sub>2</sub>O, dried with Na<sub>2</sub>SO<sub>4</sub>, filtered, and the solvent removed *in vacuo*. The material was purified by column chromatography (silica) and recrystallised from CDCl<sub>3</sub>/MeOH to afford purple crystals.

### Synthesis of compounds and characterisation data

**endo-Linker (mixture of *syn*-6a + *anti*-6b).** A solution of *endo*-cyclobutene diester anhydride **4**<sup>15,55</sup> (3.73 g, 12.2 mmol) and 2,3,5,6-tetramethyl-*p*-phenylenediamine **5** (1.0 g, 6.1 mmol, 0.5 eq.) in degassed dry DMSO (60 mL) was heated at 80 °C under an argon atmosphere for 1 day. The DMSO was removed by distillation under reduced pressure, the mixture redissolved in Ac<sub>2</sub>O (80 mL), NaOAc (7.2 g, 53 mmol) added, and the solution heated at 80 °C under a nitrogen atmosphere for a further 1 day, after which a precipitate was observed. Preliminary <sup>1</sup>H NMR of the reaction mixture suggested two isomers in an approximately 60:40 ratio (although may be due to different solubility), distinguished by outer and inner pairs of non-equivalent CH<sub>3</sub> phenyl substituent resonances. The precipitate was removed by filtration and the solids redissolved in CHCl<sub>3</sub> (200 mL), washed with H<sub>2</sub>O (2 × 200 mL), aqueous NaOH solution (2 M, 3 × 200 mL), aqueous HCl solution (2 M, 1 × 100 mL), H<sub>2</sub>O (1 × 100 mL), dried (Na<sub>2</sub>SO<sub>4</sub>), and the solvent removed *in vacuo* to afford a white powder (3.25 g, 72%, m.p. > 300 °C). The linker was used as a mixture due to difficulty in separation of the isomers.

A small sample of the isomers was separated by column chromatography, using either of the following methods or a combination of both. Method A: silica (10% THF/CHCl<sub>3</sub>) to partially resolve isomers, if bands co-elute then silica (5% MeOH/CHCl<sub>3</sub>), followed by recrystallisation from CHCl<sub>3</sub>/MeOH, solids washed with MeOH. Method B: silica plug (EtOAc), then silica (load CHCl<sub>3</sub>, elute 50% EtOAc/CHCl<sub>3</sub>, poor solubility and precipitation on column). Unfortunately the assignment of each isomer as either *syn*- or *anti*- could not be achieved by <sup>1</sup>H NOE spectroscopy, and so are referred to by the inner and outer CH<sub>3</sub> isomer nomenclature established above.

**Inner CH<sub>3</sub> isomer.** <sup>1</sup>H NMR (600 MHz, 20 °C, CDCl<sub>3</sub>): 3.80 (s, 12H), 3.50–3.47 (m, 4H), 3.11 (s, 4H), 2.98–2.95 (m, 4H), 2.07 (s, 6H), 1.95 (s, 6H), 1.86 (d, *J* = 11.6 Hz, 2H), 1.59 (d, *J* = 11.6 Hz, 2H). <sup>13</sup>C NMR (150 MHz, CDCl<sub>3</sub>): 175.72, 160.80, 141.45, 133.16, 132.62, 132.04, 52.27, 48.16, 43.15, 36.53, 34.83, 16.18, 15.51. HRMS (ESI-TOF-MS) for C<sub>40</sub>H<sub>40</sub>N<sub>2</sub>O<sub>12</sub>Na<sup>+</sup> [*M* + Na]<sup>+</sup>: calc.: 763.2479. Found: 763.2494.

**Outer CH<sub>3</sub> isomer.** <sup>1</sup>H NMR (600 MHz, 20 °C, CDCl<sub>3</sub>): 3.80 (s, 12H), 3.50–3.46 (m, 4H), 3.12 (s, 4H), 2.98–2.96 (m, 4H), 2.09 (s, 6H), 1.94 (s, 6H), 1.86 (d, *J* = 11.5 Hz, 2H), 1.59 (d, *J* = 11.5 Hz, 2H). <sup>13</sup>C NMR (150 MHz, CDCl<sub>3</sub>): 175.74, 160.79, 141.45, 133.11, 132.71, 132.03, 52.27, 48.18, 43.15, 36.55, 34.84, 16.17, 15.58. HRMS (ESI-TOF-MS) for C<sub>40</sub>H<sub>40</sub>N<sub>2</sub>O<sub>12</sub>Na<sup>+</sup> [*M* + Na]<sup>+</sup>: calc.: 763.2479. Found: 763.2494.

**endo-Bis-epoxide linker (*syn*- + *anti*-mixture **7**).** *endo*-Mitsudo linker (mixture of **6a** + **6b**) (1.50 g, 2.0 mmol) was dissolved in dry CH<sub>2</sub>Cl<sub>2</sub> (75 mL) under a nitrogen atmosphere

and cooled to 0 °C. Anhydrous *tert*-butyl hydroperoxide in toluene<sup>126</sup> (3.3 M, 1.53 mL, 5.1 mmol, 2.5 eq.) was added and stirred for a further 10 min at 0 °C, after which sublimed potassium *tert*-butoxide (0.23 g, 2.0 mmol, 1 eq.) was added. The mixture was allowed to warm to room temperature over 30 minutes, and after stirring at room temperature for a further 3 hours, the mixture was diluted with CH<sub>2</sub>Cl<sub>2</sub> (50 mL) and sodium sulfite (10% aqueous solution, 10 mL) added with vigorous stirring for 15 minutes. The mixture was further diluted with CHCl<sub>3</sub> (1 L), washed with brine (500 mL), dried with Na<sub>2</sub>SO<sub>4</sub>, filtered, and the solvent removed *in vacuo*. NMR of the reaction mixture indicated approximately 50% remaining starting material, and so the reaction was repeated on this mixture using the same quantities of epoxidation reagents (for later repeats of this reaction, the epoxidation reagent quantity was doubled from the beginning). This afforded a white powder (0.80 g, 51%), used in subsequent reactions without further purification and as a mixture of isomers. A sample was recrystallised from CHCl<sub>3</sub>/hexane for MS and melting point analysis (mixture of isomers). M.p. > 250–300 °C (decomposition). <sup>1</sup>H NMR (600 MHz, 20 °C, CDCl<sub>3</sub>): as mixture of isomers 3.82 (s, 12H), 3.46–3.41 (m, 8H), 2.74–2.70 (m, 4H), 2.24 (d, *J* = 11.2 Hz, 2H), 2.03 (a) + 2.00 (b) (singlets, combined integration 6H), 1.92 (b) + 1.89 (a) (singlets, combined integration 6H), 1.84 (d, *J* = 11.2 Hz, 2H). HRMS (ESI-TOF-MS) for C<sub>40</sub>H<sub>40</sub>N<sub>2</sub>O<sub>14</sub>Na<sup>+</sup> [*M* + Na]<sup>+</sup>: calc.: 795.2377. Found: 795.2393.

**Free base tweezer (mixture of *syn*-9a + *anti*-9b).** A suspension of *endo*-bis-epoxide linker mixture **7** (0.2 g, 0.26 mmol) and *exo*-imide porphyrin receptor **8** (0.4 g, 0.52 mmol, 2 eq.) in dry THF (10 mL) was heated in a sealed tube at 160 °C for 20–24 hours using the general procedure specified above. This procedure was repeated several times on a similar scale until 1.0 g epoxide had been reacted. The material from each reaction was combined. The solvent was removed *in vacuo* and the material purified by column chromatography (silica, 10% THF/CH<sub>2</sub>Cl<sub>2</sub>), recovering *exo*-imide porphyrin receptor **8** in the first major porphyrin band. The subsequent two closely eluting porphyrin bands each contained a majority of each isomer, and each isomer was resubjected to column chromatography to further improve separation. Isomers could be speculated as *syn*- and *anti*- on the basis of desymmetrisation of the porphyrin aromatic resonances (significant for *syn*-) and quantified by the difference in relative integrations of the inner pyrrole resonances. This afforded a purple powder (combined isomer mass 0.68 g, 23% = 10% *syn*- + 13% *anti*-). The *anti*-isomer was isolated completely free of *syn*-, while the *syn*-isomer contained approx. 25% residual *anti*-. Each isomer was crudely recrystallised from CDCl<sub>3</sub>/MeOH, however, further purification (particularly removal of the *anti*-9b isomer from the *syn*-9a sample) was carried out post-zinc(II) metalation in an effort to conserve product.

***anti*-9b.** <sup>1</sup>H NMR (600 MHz, 20 °C, CDCl<sub>3</sub>): 8.85 (s, 16H), 8.30 (d, *J* = 8.1 Hz, 4H), 8.25–8.18 (m, 12H), 7.82–7.73 (m, 18H), 7.62 (d, *J* = 8.1 Hz, 4H), 3.98 (s, 12H), 3.34–3.30 (m, 4H), 2.92 (s, 4H), 2.90 (s, 4H), 2.85–2.82 (m, 4H), 2.76 (d, *J* = 10.9 Hz, 2H), 2.58–2.51 (m, 6H, two overlapping signals), 2.32 (s,



4H), 2.28 (s, 6H), 2.04 (s, 6H), 1.41 (d,  $J = 10.9$  Hz, 2H), 1.22 (d,  $J = 11.9$  Hz, 2H),  $-2.80$  (s, 4H).

**syn-9a.** Characterised as the zinc(II) derivative.  $^1\text{H}$  NMR spectrum provided in S8† as mixture with **anti-9b**.

HRMS (ESI-TOF-MS) for two samples containing different ratios of **syn-9a/anti-9b**. Sample 1  $[\text{C}_{146}\text{H}_{116}\text{N}_{12}\text{O}_{18}]^{2+}$   $[\text{M} + 2\text{H}]^{2+}$ : calc.: 1162.4260. Found: 1162.4267. Sample 2  $[\text{C}_{146}\text{H}_{114}\text{N}_{12}\text{O}_{18}\text{Na}_2]^{2+}$   $[\text{M} + 2\text{Na}]^{2+}$ : calc.: 1184.4079. Found: 1184.4110.

**syn-Zinc(II) tweezer, 3a.**  $\text{Zn}(\text{OAc})_2 \cdot 2\text{H}_2\text{O}$  (1.0 g, 4.55 mmol) in MeOH (10 mL) was heated under reflux with **syn-9a** (mixture with 25% **anti-9b**, 0.37 g, 0.16 mmol) in  $\text{CH}_2\text{Cl}_2$  (20 mL), during which the solution developed a green/blue hue, and was worked up according to the general procedure above. The product was purified by column chromatography to remove the green/blue impurity (silica, 10% THF/ $\text{CHCl}_3$ ) collecting the strong porphyrin band. The solvent was removed *in vacuo* to afford a purple powder (0.31 g, 79%), in which remained 33% **anti**-isomer (determined by relative NMR integration). This material was recrystallised repeatedly from  $\text{CHCl}_3/\text{MeOH}$  until free of the **anti**-isomer (approximately three to four times), to afford bright purple crystals for host-guest titrations.  $^1\text{H}$  NMR (600 MHz, 20 °C,  $\text{CDCl}_3$ , approx. 1 mM, concentration dependent): 8.93–8.84 (m, 16H), 8.23–8.16 (m, 8H), 8.14–8.09 (m, 8H), 7.78–7.70 (m, 6H), 7.66–7.60 (m, 12H), 7.48–7.38 (bs, 4H), 3.98 (s, 12H), 3.33 (m, 4H), 2.88–2.83 (m, 8H), 2.81 (s, 4H), 2.77 (d,  $J = 11.1$  Hz, 2H), 2.56 (s, 4H), 2.49 (d,  $J = 11.9$  Hz, 2H), 2.33 (s, 4H), 2.31 (s, 6H), 2.00 (s, 6H), 1.43 (d,  $J = 11.1$  Hz, 2H), 1.13 (d,  $J = 11.9$  Hz, 2H). UV/Vis ( $\text{CHCl}_3$ ):  $\lambda_{\text{max}}$  (nm) = 418.4 (shoulder around 400), 547.3, 583.9,  $\epsilon_{\text{single porphyrin}} = 4.9 \times 10^5 \text{ L mol}^{-1} \text{ cm}^{-1}$ . HRMS (MALDI-TOF) for  $\text{C}_{146}\text{H}_{110}\text{N}_{12}\text{O}_{18}\text{Zn}_2$   $[\text{M}]^{+}$ : calc.: 2446.664 (monoisotopic). Found: 2446.694.

**anti-Zinc(II) tweezer, 3b.**  $\text{Zn}(\text{OAc})_2 \cdot 2\text{H}_2\text{O}$  (1.0 g, 4.55 mmol) in MeOH (10 mL) was heated under reflux with **anti-9b** (0.31 g, 0.13 mmol) in  $\text{CH}_2\text{Cl}_2$  (20 mL) and worked up according to the general procedure above. The product was purified by column chromatography (silica, 10% THF/ $\text{CHCl}_3$ ) collecting the strong porphyrin band. The solvent was removed *in vacuo* to afford a purple powder (0.29 g, 89%), which was recrystallised from  $\text{CHCl}_3/\text{MeOH}$  to afford bright purple crystals (free from **syn**-isomer) for host-guest titrations.  $^1\text{H}$  NMR (600 MHz, 20 °C,  $\text{CDCl}_3$ , approx. 0.85 mM): 8.97–8.94 (m, 16H), 8.31 (d,  $J = 8.2$  Hz, 4H), 8.24–8.20 (m, 12 H), 7.81–7.73 (m, 18H), 7.61 (d,  $J = 8.2$  Hz, 4H), 3.98 (s, 12H), 3.33 (m, 4H), 2.91 (s, 4H), 2.89 (s, 4H), 2.84 (m, 4H), 2.77 (d,  $J = 10.8$  Hz, 2H), 2.58–2.50 (m, 6H, two overlapping signals), 2.32 (s, 4H), 2.28 (s, 6H), 2.04 (s, 6H), 1.42 (d,  $J = 10.8$  Hz, 2H), 1.22 (d,  $J = 12.2$  Hz, 2H). UV/Vis ( $\text{CHCl}_3$ ):  $\lambda_{\text{max}}$  (nm) = 399.2 (shoulder), 419.3, 547.4, 585.8,  $\epsilon_{\text{single porphyrin}} = 5.8 \times 10^5 \text{ L mol}^{-1} \text{ cm}^{-1}$ . HRMS (MALDI-TOF) for  $\text{C}_{146}\text{H}_{110}\text{N}_{12}\text{O}_{18}\text{Zn}_2$   $[\text{M}]^{+}$ : calc.: 2446.6644 (monoisotopic). Found: 2446.6770.

**exo-Linker analogues (syn-11a + anti-11b).** A solution of *cis*-5-norbornene-*exo*-2,3-dicarboxylic anhydride<sup>127</sup> (3.0 g, 18.3 mmol) and 2,3,5,6-tetramethyl-*p*-phenylenediamine 5 (1.5 g, 9.1 mmol, 0.5 eq.) in degassed dry DMF (50 mL) was heated at 80 °C under an argon atmosphere for 3 days, during

which a white precipitate formed. The mixture was filtered, washed with hexane, the solid redissolved in  $\text{Ac}_2\text{O}$  (50 mL), NaOAc (5.0 g, 36.7 mmol) added, and the mixture heated at 80 °C under a nitrogen atmosphere for a further 3 days. Any precipitate was removed by filtration, and the precipitate and  $\text{Ac}_2\text{O}$  filtrate separately purified. The precipitate was washed with hexane ( $2 \times 100$  mL), redissolved in  $\text{CHCl}_3$  (100 mL), washed with  $\text{H}_2\text{O}$  ( $2 \times 100$  mL), dried with  $\text{Na}_2\text{SO}_4$ , and the solvent removed *in vacuo* to afford a solid. For the  $\text{Ac}_2\text{O}$  filtrate, the  $\text{Ac}_2\text{O}$  was removed by distillation under reduced pressure, the solid washed with hexane ( $2 \times 100$  mL), redissolved in  $\text{CHCl}_3$  (100 mL), washed with  $\text{H}_2\text{O}$  ( $2 \times 100$  mL), dried with  $\text{Na}_2\text{SO}_4$ , and the solvent removed *in vacuo* to afford a solid.  $^1\text{H}$  NMR of the filtrate and precipitate show that each contains a majority of the opposite isomer, **syn**- or **anti**-, distinguished by outer and inner pairs of non-equivalent  $\text{CH}_3$  phenyl substituent resonances. Additionally, X-ray crystallographic analysis of crystals from both the filtrate and precipitate fractions enabled assignment of the **syn**- and **anti**-isomers.

**syn-11a (filtrate, outer  $\text{CH}_3$ ).** M.p. > 300 °C (crystals crack, partial decomposition).  $^1\text{H}$  NMR (600 MHz, 20 °C,  $\text{CDCl}_3$ ): 6.34 (m, 4H), 3.42 (m, 4H), 2.91 (s, 4H), 2.051 (s, 6H), 1.967 (s, 6H), 1.68 (m, 4H).  $^{13}\text{C}$  NMR (150 MHz,  $\text{CHCl}_3$ ): 176.72, 138.03, 133.08, 132.67, 131.86, 48.47, 45.29, 43.80, 15.90, 15.63. HRMS (ESI-TOF-MS) for  $\text{C}_{28}\text{H}_{28}\text{N}_2\text{O}_4\text{Na}^+$   $[\text{M} + \text{Na}]^+$ : calc.: 479.1947. Found: 479.1957. Single crystal for X-ray diffraction analysis was grown from  $\text{CH}_3\text{CN}$  by slow evaporation. CCDC 1526930† contains the supplementary crystallographic data for this paper.

**anti-11b (precipitate, inner  $\text{CH}_3$ ).** M.p. > 300 °C (crystals transition from clear to white 195–205 °C, partial decomposition by 300 °C).  $^1\text{H}$  NMR (600 MHz, 20 °C,  $\text{CDCl}_3$ ): 6.34 (m, 4H), 3.42 (m, 4H), 2.91 (s, 4H), 2.039 (s, 6H), 1.973 (s, 6H), 1.67 (m, 4H).  $^{13}\text{C}$  NMR (150 MHz,  $\text{CHCl}_3$ ): 176.70, 138.01, 133.14, 132.58, 131.84, 48.46, 45.28, 43.78, 15.99, 15.50. HRMS (ESI-TOF-MS) for  $\text{C}_{28}\text{H}_{28}\text{N}_2\text{O}_4\text{Na}^+$   $[\text{M} + \text{Na}]^+$ : calc.: 479.1947. Found: 479.1949. Single crystal for X-ray diffraction analysis was grown from  $\text{CH}_3\text{CN}$  by slow evaporation, and solved as the structure co-crystallised with approx. 6% mono-epoxide (at the norbornene). CCDC 1526931† contains the supplementary crystallographic data for this paper.

## Conflicts of interest

There are no conflicts to declare.

## Acknowledgements

R. B. M wishes to thank Flinders University for the provision of an Australian Postgraduate Award and the Playford Memorial Trust for a PhD top-up scholarship. R. B. M also thanks the following for their efforts and expertise in accurate mass spectrometry: Dr Sally Duck (Monash University) porphyrin compound 9, Dr Craig Brinkworth (Defence Science





and Technology Group, Australia) porphyrin compounds **syn-3a** and **anti-3b**, Dr Daniel Jardine (Flinders Analytical) all other compounds.

## Notes and references

- J. W. Steed and J. L. Atwood, *Supramolecular Chemistry*, John Wiley & Sons, Ltd, 1st edn, 2000.
- D. Cram, *Science*, 1988, **240**, 760–767.
- D. J. Cram, G. M. Lein, T. Kaneda, R. C. Helgeson, C. B. Knobler, E. Maverick and K. N. Trueblood, *J. Am. Chem. Soc.*, 1981, **103**, 6228–6232.
- V. Valderrey, G. Aragay and P. Ballester, *Coord. Chem. Rev.*, 2014, **258–259**, 137–156.
- S. Otto, *Dalton Trans.*, 2006, 2861–2864.
- N. Voyer and F. Maltais, *Adv. Mater.*, 1993, **5**, 568–570.
- S. P. Gaynor, M. J. Gunter, M. R. Johnston and R. N. Warrener, *Org. Biomol. Chem.*, 2006, **4**, 2253–2266.
- M. Nakash and J. K. M. Sanders, *J. Org. Chem.*, 2000, **65**, 7266–7271.
- Z. Rodriguez-Docampo, E. Eugenieva-Ilieva, C. Reyheller, A. M. Belenguer, S. Kubik and S. Otto, *Chem. Commun.*, 2011, **47**, 9798–9800.
- H. Sun, C. A. Hunter and E. M. Llamas, *Chem. Sci.*, 2015, **6**, 1444–1453.
- L. Pengpeng, P. Neuhaus, D. V. Kondratuk, T. S. Balaban and H. L. Anderson, *Angew. Chem., Int. Ed.*, 2014, **53**, 7770–7773.
- N. Solladié, S. Bouatra, R. Rein and J. Roeser, *J. Porphyrins Phthalocyanines*, 2005, **9**, 779–787.
- N. Solladié, F. Aziat, S. Bouatra and R. Rein, *J. Porphyrins Phthalocyanines*, 2008, **12**, 1250–1260.
- S. Merkas, S. Bouatra, R. Rein, I. Piantanida, M. Zinic and N. Solladié, *J. Porphyrins Phthalocyanines*, 2015, **19**, 535–546.
- R. B. Murphy, D.-T. Pham, S. F. Lincoln and M. R. Johnston, *Eur. J. Org. Chem.*, 2013, 2985–2993.
- H. L. Anderson, S. Anderson and J. K. M. Sanders, *J. Chem. Soc., Perkin Trans. 1*, 1995, 2231–2245.
- J. Etchebarria, A. Vidal-Ferran and P. Ballester, *Chem. Commun.*, 2008, 5939–5941.
- N. Solladié, N. Aubert, S. Bouatra, C. Bourgogne, F. Bregier, J. Brettar, J.-P. Gisselbrecht, M. Gross, R. Rein, C. Sooambar, V. Troiani and M. Walther, *J. Porphyrins Phthalocyanines*, 2003, **7**, 270–281.
- M. R. Johnston and D. M. Lyons, *Supramol. Chem.*, 2005, **17**, 503–511.
- D. Kim, S. Lee, G. Gao, H. S. Kang and J. Ko, *J. Organomet. Chem.*, 2009, **695**, 111–119.
- Y. Kubo, Y. Murai, J.-i. Yamanaka, S. Tokita and Y. Ishimaru, *Tetrahedron Lett.*, 1999, **40**, 6019–6023.
- S. Yagi, M. Ezoe, I. Yonekura, T. Takagishi and H. Nakazumi, *J. Am. Chem. Soc.*, 2003, **125**, 4068–4069.
- L. H. Tong, J.-L. Wietor, W. Clegg, P. R. Raithby, S. I. Pascu and J. K. M. Sanders, *Chem. – Eur. J.*, 2008, **14**, 3035–3044.
- C.-H. Lee, H. Yoon and W.-D. Jang, *Chem. – Eur. J.*, 2009, **15**, 9972–9976.
- M. Dudič, P. Lhoták, H. Petříčková, I. Stibor, K. Lang and J. Sýkora, *Tetrahedron*, 2003, **59**, 2409–2415.
- D. Jokic, Z. Asfari and J. Weiss, *Org. Lett.*, 2002, **4**, 2129–2132.
- D. Jokic, C. Boudon, G. Pognon, M. Bonin, K. J. Schenk, M. Gross and J. Weiss, *Chem. – Eur. J.*, 2005, **11**, 4199–4209.
- P. Mondal and S. P. Rath, *Isr. J. Chem.*, 2016, **56**, 144–155.
- M. Blom, S. Norrehed, C.-H. Andersson, H. Huang, M. Light, J. Bergquist, H. Grennberg and A. Gogoll, *Molecules*, 2016, **21**, 16.
- R. B. Murphy, R. E. Norman, J. M. White, M. V. Perkins and M. R. Johnston, *Org. Biomol. Chem.*, 2016, **14**, 8707–8720.
- R. N. Warrener, D. N. Butler, W. Y. Liao, I. G. Pitt and R. A. Russell, *Tetrahedron Lett.*, 1991, **32**, 1889–1892.
- R. N. Warrener, I. G. Pitt and D. N. Butler, *J. Chem. Soc., Chem. Commun.*, 1983, 1340–1342.
- R. N. Warrener, A. C. Schultz, D. N. Butler, S. Wang, I. B. Mahadevan and R. A. Russell, *Chem. Commun.*, 1997, 1023–1024.
- R. N. Warrener, S. Wang and R. A. Russell, *Tetrahedron*, 1997, **53**, 3975–3990.
- R. N. Warrener, D. N. Butler, D. Margetic, F. M. Pfeffer and R. A. Russell, *Tetrahedron Lett.*, 2000, **41**, 4671–4675.
- M. Golić, M. R. Johnston, D. Margetić, A. C. Schultz and R. N. Warrener, *Aust. J. Chem.*, 2006, **59**, 899–914.
- D. Margetic, M. R. Johnston, E. R. T. Tiekink and R. N. Warrener, *Tetrahedron Lett.*, 1998, **39**, 5277–5280.
- R. N. Warrener, D. N. Butler, L. Liu, D. Margetic and R. A. Russell, *Chem. – Eur. J.*, 2001, **7**, 3406–3414.
- M. J. Gunter, H. Tang and R. N. Warrener, *J. Porphyrins Phthalocyanines*, 2002, **6**, 673–684.
- A. M. Napper, I. Read, N. J. Head, A. M. Oliver and M. N. Paddon-Row, *J. Am. Chem. Soc.*, 2000, **122**, 5220–5221.
- N. J. Head, A. M. Oliver, K. Look, N. R. Lokan, G. A. Jones and M. N. Paddon-Row, *Angew. Chem., Int. Ed.*, 1999, **38**, 3219–3222.
- M. J. Shephard and M. N. Paddon-Row, *J. Phys. Chem. A*, 2000, **104**, 11628–11635.
- M. J. Shephard and M. N. Paddon-Row, *J. Phys. Chem. A*, 1999, **103**, 3347–3350.
- M. R. Johnston, M. J. Latter and R. N. Warrener, *Org. Lett.*, 2002, **4**, 2165–2168.
- M. Johnston, *Molecules*, 2001, **6**, 406–416.
- M. R. Johnston, M. J. Latter and R. N. Warrener, *Aust. J. Chem.*, 2001, **54**, 633–636.
- M. D. Johnstone, E. K. Schwarze, J. Ahrens, D. Schwarzer, J. J. Holstein, B. Dittrich, F. M. Pfeffer and G. H. Clever, *Chem. – Eur. J.*, 2016, **22**, 10791–10795.
- M. D. Johnstone, M. Frank, G. H. Clever and F. M. Pfeffer, *Eur. J. Org. Chem.*, 2013, 5848–5853.
- R. N. Robson and F. M. Pfeffer, *Chem. Commun.*, 2016, **52**, 8719–8721.





- 50 M. D. Johnstone, E. K. Schwarze, G. H. Clever and F. M. Pfeffer, *Chem. – Eur. J.*, 2015, **21**, 3948–3955.
- 51 A. J. Lowe, B. M. Long and F. M. Pfeffer, *Chem. Commun.*, 2013, **49**, 3376–3388.
- 52 B. M. Long and F. M. Pfeffer, *Chem. – Asian J.*, 2014, **9**, 1091–1098.
- 53 R. N. Robson, B. P. Hay and F. M. Pfeffer, *ChemistrySelect*, 2017, **2**, 4605–4608.
- 54 G. H. Clever and P. Punt, *Acc. Chem. Res.*, 2017, **50**, 2233–2243.
- 55 M. Shang, R. N. Warrener, D. N. Butler, Y. Murata and D. Margetić, *Mol. Diversity*, 2011, **15**, 541–560.
- 56 P. Trošelj, A. Briš, Y. Murata and D. Margetić, *Struct. Chem.*, 2012, **23**, 791–799.
- 57 P. Trošelj, I. Đilović, D. Matković-Čalogović and D. Margetić, *J. Heterocycl. Chem.*, 2013, **50**, 83–90.
- 58 H. Tang, Z. Dong, Z. Merican, D. Margetić, Ž. Marinić, M. J. Gunter, D. Officer, D. N. Butler and R. N. Warrener, *Tetrahedron Lett.*, 2009, **50**, 667–670.
- 59 A. R. Mulholland, P. Thordarson, E. J. Mensforth and S. J. Langford, *Org. Biomol. Chem.*, 2012, **10**, 6045–6053.
- 60 G. Giancane, V. Borovkov, Y. Inoue and L. Valli, *J. Colloid Interface Sci.*, 2012, **385**, 282–284.
- 61 V. V. Borovkov, J. M. Lintuluoto and Y. Inoue, *Tetrahedron Lett.*, 1999, **40**, 5051–5054.
- 62 V. V. Borovkov, J. M. Lintuluoto and Y. Inoue, *J. Phys. Chem. B*, 1999, **103**, 5151–5156.
- 63 V. V. Borovkov, J. M. Lintuluoto and Y. Inoue, *J. Am. Chem. Soc.*, 2001, **123**, 2979–2989.
- 64 R. N. Warrener, M. R. Johnston and M. J. Gunter, *Synlett*, 1998, 593–595.
- 65 R. C. Foitzik, A. Lowe and F. M. Pfeffer, *Tetrahedron Lett.*, 2009, **50**, 2583–2584.
- 66 J.-H. Fuhrhop and K. M. Smith, *Laboratory methods in porphyrin and metalloporphyrin research*, Elsevier Scientific Pub. Co., 1975.
- 67 E. Stulz, C. C. Mak and J. K. M. Sanders, *J. Chem. Soc., Dalton Trans.*, 2001, 604–613.
- 68 M. Kasha, H. R. Rawls and M. A. El-Bayoumi, *Pure Appl. Chem.*, 1965, **11**, 371–392.
- 69 A. Osuka and K. Maruyama, *J. Am. Chem. Soc.*, 1988, **110**, 4454–4456.
- 70 C. A. Hunter, J. K. M. Sanders and A. J. Stone, *Chem. Phys.*, 1989, **133**, 395–404.
- 71 C. K. Chang and I. Abdalmuhdi, *J. Org. Chem.*, 1983, **48**, 5388–5390.
- 72 H. A. Staab and T. Carell, *Angew. Chem., Int. Ed. Engl.*, 1994, **33**, 1466–1468.
- 73 Y. Yu, L. Shi, D. Yang and L. Gan, *Chem. Sci.*, 2013, **4**, 814–818.
- 74 S. Verma and N. Singh, *Aust. J. Chem.*, 1976, **29**, 295–300.
- 75 D. P. Curran, S. Geib and N. DeMello, *Tetrahedron*, 1999, **55**, 5681–5704.
- 76 K. Tanaka, M. Okano, H. Toshino, H. Kita and K.-I. Okamoto, *J. Polym. Sci., Part B: Polym. Phys.*, 1992, **30**, 907–914.
- 77 Y. Zhang, J. M. Lavin and K. D. Shimizu, *J. Am. Chem. Soc.*, 2009, **131**, 12062–12063.
- 78 D.-S. Choi, Y. S. Chong, D. Whitehead and K. D. Shimizu, *Org. Lett.*, 2001, **3**, 3757–3760.
- 79 Y. Chen, M. D. Smith and K. D. Shimizu, *Tetrahedron Lett.*, 2001, **42**, 7185–7187.
- 80 R. D. Rasberry, X. Wu, B. N. Bullock, M. D. Smith and K. D. Shimizu, *Org. Lett.*, 2009, **11**, 2599–2602.
- 81 C. F. Degenhardt, J. M. Lavin, M. D. Smith and K. D. Shimizu, *Org. Lett.*, 2005, **7**, 4079–4081.
- 82 J. M. Lavin and K. D. Shimizu, *Chem. Commun.*, 2007, 228–230.
- 83 W. R. Carroll, P. Pellechia and K. D. Shimizu, *Org. Lett.*, 2008, **10**, 3547–3550.
- 84 C. W. Miller, C. E. Hoyle, E. J. Valente, D. H. Magers and E. S. Jönsson, *J. Phys. Chem. A*, 1999, **103**, 6406–6412.
- 85 K. Kondo, H. Fujita, T. Suzuki and Y. Murakami, *Tetrahedron Lett.*, 1999, **40**, 5577–5580.
- 86 M. Mao, J. England and S. R. Turner, *Polymer*, 2011, **52**, 4498–4502.
- 87 C. W. Miller, E. S. Jönsson, C. E. Hoyle, K. Viswanathan and E. J. Valente, *J. Phys. Chem. B*, 2001, **105**, 2707–2717.
- 88 C. Miller, C. Hoyle, E. Valente, J. Zubkowski and E. S. Jönsson, *J. Chem. Crystallogr.*, 2000, **30**, 563–571.
- 89 D. P. Curran and N. C. DeMello, *J. Chem. Soc., Chem. Commun.*, 1993, 1314–1317.
- 90 R. B. Murphy, PhD thesis, Flinders University, Adelaide, South Australia, 2016.
- 91 *Mercury 3.8*, CCDC, 2016, <http://www.ccdc.cam.ac.uk/mercury/>.
- 92 P. D. Bartlett, G. L. Combs, A. X. T. Le, W. H. Watson, J. Galloy and M. Kimura, *J. Am. Chem. Soc.*, 1982, **104**, 3131–3138.
- 93 *Spartan '10 for Windows*, Wavefunction, Inc., 18401 Von Karman Avenue, Suite 370, Irvine, CA 92612 USA, <http://www.wavefun.com/index.html>.
- 94 B. A. Langowski, R. Rothchild and A.-M. Sapse, *Spectrosc. Lett.*, 2001, **34**, 235–251.
- 95 A. Camara-Campos, C. A. Hunter and S. Tomas, *Proc. Natl. Acad. Sci. U. S. A.*, 2006, **103**, 3034–3038.
- 96 P. N. Taylor and H. L. Anderson, *J. Am. Chem. Soc.*, 1999, **121**, 11538–11545.
- 97 H.-T. Nguyen, D.-T. Pham, C. J. Easton and S. F. Lincoln, *Aust. J. Chem.*, 2013, **66**, 1057–1064.
- 98 E. A. Kataev and T. A. Shumilova, *Molecules*, 2015, **20**, 3354–3370.
- 99 R. Montis, M. C. Aragoni, M. Arca, C. Bazzicalupi, A. J. Blake, C. Caltagirone, G. De Filippo, A. Garau, P. Gratteri, F. Isaia, V. Lippolis and A. Pintus, *Inorg. Chim. Acta*, 2012, **381**, 170–180.
- 100 F. Ulatowski, K. Dąbrowa, T. Bałakier and J. Jurczak, *J. Org. Chem.*, 2016, **81**, 1746–1756.
- 101 S. A. Ikbāl, S. Brahma and S. P. Rath, *Chem. Commun.*, 2015, **51**, 895–898.
- 102 A. Dhamija, S. A. Ikbāl and S. P. Rath, *Inorg. Chem.*, 2016, **55**, 13014–13026.



- 103 E. A. Kataev, N. Backmann, T. A. Shumilova, T. Rüffer and H. Lang, *Supramol. Chem.*, 2016, **28**, 53–61.
- 104 *Protonic Software*, 2 Templegate Avenue, Leeds, LS150HD, UK. (<http://www.hyperquad.co.uk>).
- 105 P. Gans, A. Sabatini and A. Vacca, *Talanta*, 1996, **43**, 1739–1753.
- 106 P. Ballester, A. Costa, A. M. Castilla, P. M. Deyà, A. Frontera, R. M. Gomilla and C. A. Hunter, *Chem. – Eur. J.*, 2005, **11**, 2196–2206.
- 107 L. Baldini, P. Ballester, A. Casnati, R. M. Gomila, C. A. Hunter, F. Sansone and R. Ungaro, *J. Am. Chem. Soc.*, 2003, **125**, 14181–14189.
- 108 P. Ballester, A. I. Oliva, A. Costa, P. M. Deyà, A. Frontera, R. M. Gomila and C. A. Hunter, *J. Am. Chem. Soc.*, 2006, **128**, 5560–5569.
- 109 H. L. Anderson, *Inorg. Chem.*, 1994, **33**, 972–981.
- 110 C. C. Mak, N. Bampos and J. M. K. Sanders, *Angew. Chem., Int. Ed.*, 1998, **37**, 3020–3023.
- 111 C. A. Hunter, M. N. Meah and J. K. M. Sanders, *J. Am. Chem. Soc.*, 1990, **112**, 5773–5780.
- 112 H. L. Anderson, C. A. Hunter, M. N. Meah and J. K. M. Sanders, *J. Am. Chem. Soc.*, 1990, **112**, 5780–5789.
- 113 S. S. Eaton and G. R. Eaton, *J. Chem. Soc., Chem. Commun.*, 1974, 576–577.
- 114 R. W. Wagner, T. E. Johnson and J. S. Lindsey, *J. Am. Chem. Soc.*, 1996, **118**, 11166–11180.
- 115 S. S. Eaton and G. R. Eaton, *J. Am. Chem. Soc.*, 1975, **97**, 3660–3666.
- 116 R. Dennington, T. Keith and J. Millam, *GaussView, Version 5.0.9*, Semichem Inc., Shawnee Mission, KS, 2009.
- 117 G. Ercolani and L. Schiaffino, *Angew. Chem., Int. Ed.*, 2011, **50**, 1762–1768.
- 118 C. A. Hunter and H. L. Anderson, *Angew. Chem., Int. Ed.*, 2009, **48**, 7488–7499.
- 119 H. J. Hogben, J. K. Sprafke, M. Hoffmann, M. Pawlicki and H. L. Anderson, *J. Am. Chem. Soc.*, 2011, **133**, 20962–20969.
- 120 M. Strohm, *mMass 5.4.1*, 2012 <http://www.mmass.org/>.
- 121 H. E. Gottlieb, V. Kotlyar and A. Nudelman, *J. Org. Chem.*, 1997, **62**, 7512–7515.
- 122 G. Sheldrick, *Acta Crystallogr., Sect. A: Found. Crystallogr.*, 2008, **64**, 112–122.
- 123 L. Farrugia, *J. Appl. Crystallogr.*, 1997, **30**, 565.
- 124 L. Farrugia, *J. Appl. Crystallogr.*, 1999, **32**, 837–838.
- 125 D. D. Perrin, L. Armarego and D. R. Perrin, *Purification of Laboratory Chemicals*, Pergamon Press, Ltd., Oxford, 1966.
- 126 J. G. Hill, B. E. Rossiter and K. B. Sharpless, *J. Org. Chem.*, 1983, **48**, 3607–3608.
- 127 D. Craig, *J. Am. Chem. Soc.*, 1951, **73**, 4889–4892.
- 128 G. Ercolani, C. Piguet, M. Borkovec and J. Hamacek, *J. Phys. Chem. B*, 2007, **111**, 12195–12203.

